NASA TECHNICAL NOTE

NASA TN D-5311

c. 1

NASA TN D-5311

FEASIBILITY OF DETECTING RADIATION SCATTERED FROM A PLASMA

by Melville Clark, Jr.

Electronics Research Center
Cambridge, Mass.

NATIONAL AERONAUTICS AND SPACE ADMINISTRATION • WASHINGTON, D. C. • SEPTEMBER 1969

1. Report No. NASA TN D-5311	2. Government Accession No.	3. Recipient's Catalog No.
4. Title and Subtitle Feasibility of Detecting Radiation Scattered from a Plasma		5. Report Date September 1969 6. Performing Organization Code
7. Author(s) Melville Clark, Jr.		8. Performing Organization Report No. C-65
9. Performing Organization Name and Address Electronics Research Center Cambridge, Massachusetts		10. Work Unit No. 129-02-01-05-25 11. Contract or Grant No.
12. Sponsoring Agency Name and Address National Aeronautics and Space Administration Washington D.C. 20546		13. Type of Report and Period Covered Technical Note 14. Sponsoring Agency Code

15. Supplementary Notes

16. Abstract

It is shown that it is possible to detect radiation scattered from a plasma in doppler-shifted lines. The method provides a way of measuring the fluctuation in plasma charge density.

17. Key Words •Laser •Satellite •Radiation •Frequency •Detection •Modulation •Scattering •Plasma	18. Distribution Statement Unclassified - Unlimited

19. Security Classif. (of this report)	20. Security Classif. (of this page)	21. No. of Pages	22. Price *
Unclassified	Unclassified	55	$3.00

*For sale by the Clearinghouse for Federal Scientific and Technical Information Springfield, Virginia 22151

FEASIBILITY OF DETECTING RADIATION SCATTERED FROM A PLASMA

By Melville Clark, Jr.
Electronics Research Center

SUMMARY

This theoretical study shows the feasibility of detecting laser radiation scattered from a plasma in a satellite line, this line being separated from the laser frequency by approximately the plasma frequency. The experiment may be performed at 1.06μ or 10.6μ with bremsstrahlung noise limiting the signal-to-noise ratio in the first case and thermal noise limiting this ratio in the second case. To reduce the effects of laser-radiation scattered from the walls of the vacuum chamber, both the laser radiation and plasma are modulated at different audio frequencies. A narrow, bandpass electrical filter centered at the sum frequency rejects the signal deriving directly from wall scattering of the laser radiation. A narrow, bandpass optical filter centered on the laser frequency reduces noise due to flucuations in out-of-band radiation, bremsstrahlung, and thermal radiation. A lock-in amplifier at the output of the low noise amplifier is synchronized to the sum frequency and further improves the signal-to-noise ratio.

Because more can be done to reduce thermal noise than noise due to bremsstrahlung, a wavelength of 10.6μ is preferred. In this event, liquid-helium-cooled germanium doped with either copper or mercury would be used as a detector. A low-noise field effect transistor mounted on the dewar would be used as the first stage of amplification. Likewise, the optical, narrow, bandpass filter would be mounted on the dewar just ahead of the detector in order to reduce thermal noise radiation from the filter. The radiation would, of course, be supplied by a high-power, cw, CO_2 laser, and this radiation would be modulated by chopping.

Because the electron density and temperature of the plasma are both unknown and not amenable to easy calculation, the results are studied as a function of these quantities as parameters.

INTRODUCTION

The scattering of photons from a plasma can teach several things about a plasma. The scattering is related to the fluctuation in density (ref. 1). From the properties of the scattered radiation, we can determine the temperature and density of a plasma. Accordingly, an experiment has been proposed in which

highly monochromatic photons would be scattered by a plasma. In this experiment, the cross-section for the scattering would be measured as a function of the frequency of the scattered photons. Since the experiment is quite difficult, it is our present purpose to make a feasibility study of the experimental problems.

The author acknowledges the contributions of the following scientific personnel in the preparation of this Technical Note: Allen Offenberger, Lawrence Lidsky, Kenneth Button, David Whitehouse, Brian Woodcock, Lawrence Rubin, Colin Whitney, Charles Freed, Thomas Driscoll, James Leone, and John Hobert.

THEORETICAL RESULTS

The scattering cross-section is proportional to the electron density fluctuations of the plasma (ref. 1). The electron density fluctuations of a plasma have been related to the properties of the plasma (ref. 2). In particular,

$$\left\langle \left| Q_e(\omega) \right|^2 \right\rangle = \frac{\sqrt{\pi}\, Ne^2}{\gamma} \left\{ \frac{\Gamma_\alpha(x)}{\omega_e} + Z\left(\frac{\alpha^2}{1+\alpha^2} \right)^2 \frac{\Gamma_\beta(y)}{\omega_i} \right\} , \qquad (1)$$

where

$$\Gamma_\alpha(x) = e^{-x^2} \left\{ \left[1 + \alpha^2 - \alpha^2 f(x) \right]^2 + \pi\alpha^4 x^2 e^{-2x^2} \right\}^{-1} , \qquad (2)$$

$$f(x) = 2xe^{-x^2} \int_0^x dt\, e^{t^2} , \qquad (3) \qquad x = \omega/\omega_e , \qquad (4)$$

$$y = \omega/\omega_i , \qquad (5)$$

$$\beta^2 = \frac{ZT\alpha^2}{T_i(1+\alpha^2)} , \qquad (6)$$

$$\omega_e = \sqrt{2k^2 \kappa T/m} , \qquad (7)$$

$$\omega_i = \sqrt{2k^2 \kappa T_i/M} , \qquad (8)$$

$$\alpha = 1/k\lambda_D \ , \tag{9}$$

$$k = (4\pi/\lambda)\sin(\theta/2) \ , \tag{10}$$

$$\lambda_D = \sqrt{\varepsilon\kappa T/ne^2} \ , \tag{11}$$

λ is the wavelength of the incident radiation, ε is the permittivity of vacuum, N is the number of electrons in a volume V, m is the mass, e is the charge of each electron, M is the mass of each ion, κ is Boltzmann's constant, n is the density of electrons, θ is the angle of scattering, T is the temperature of the electrons, T_i is the temperature of the ions, Z is the atomic number of the ions, and γ is the reciprocal of twice the time of observation.

The function f(x) may be approximated by a power series expansion:

$$f(x) = 2x^2\left\{1 - \frac{2}{3}x^2 + \frac{4}{15}x^4 + \ldots + \frac{(-2x^2)^n}{3.5\ \ldots(2n+1)} + \ldots\right\} \tag{12}$$

or by an asymptotic expansion

$$f(x) \sim 1 + \frac{1}{2x^2}\left\{1 + \frac{3}{2x^2} + \frac{15}{4x^4} + \ldots\right\} \ . \tag{13}$$

The function f(x) is plotted in Figure 1; $\Gamma_\alpha(x)$ is plotted in Figure 2 for several values of α. It is easily seen that $\Gamma_\alpha(x)$ is an even function of x. For this reason, we restrict all graphs and remarks to positive x. It is readily observed that $\Gamma_\alpha(x)$ has one maximum (for positive x) that becomes very sharp as α increases. We are interested in detecting the existence of this maximum and in measuring the shape of the fluctuation in the neighborhood of this maximum.

It behooves us to derive an approximate formula for α near the maximum. If $\alpha \gg 1$, then:

$$\Gamma_\alpha(x) \approx \frac{\alpha^2}{2} e^{-x_0^2}\left\{4(x - x_0)^2 + \left[\frac{\sqrt{\pi}}{2}\alpha^4 e^{-x_0^2}\right]^2\right\}^{-1} \ , \tag{14}$$

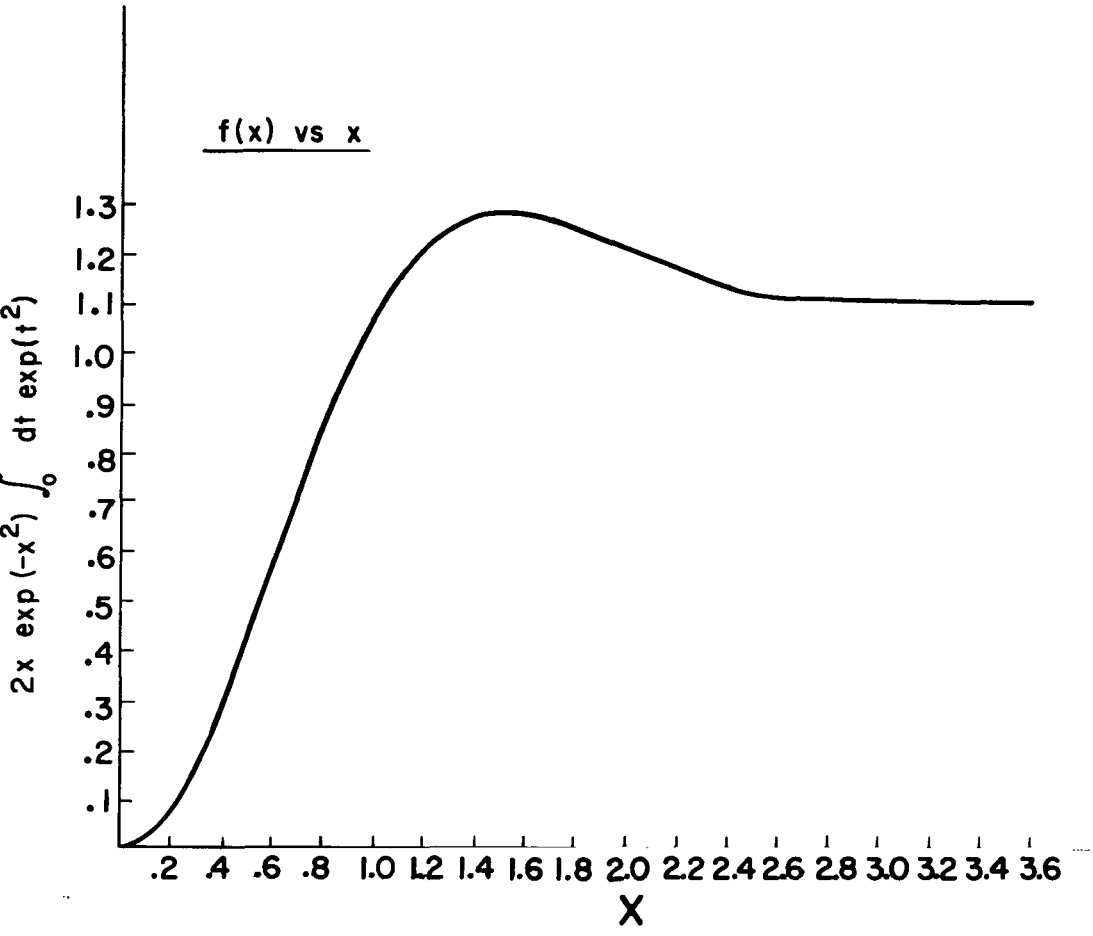

Figure 1.- The function $2x \exp(-x^2) \int_0^x dt \exp(t^2)$ vs x.

* * * * * *

where x_0 is such that:

$$f(x_0) = 1 + \frac{1}{\alpha^2} , \tag{15}$$

and

$$x_0 \approx \sqrt{\frac{\alpha^2 + 3}{2}} . \tag{16}$$

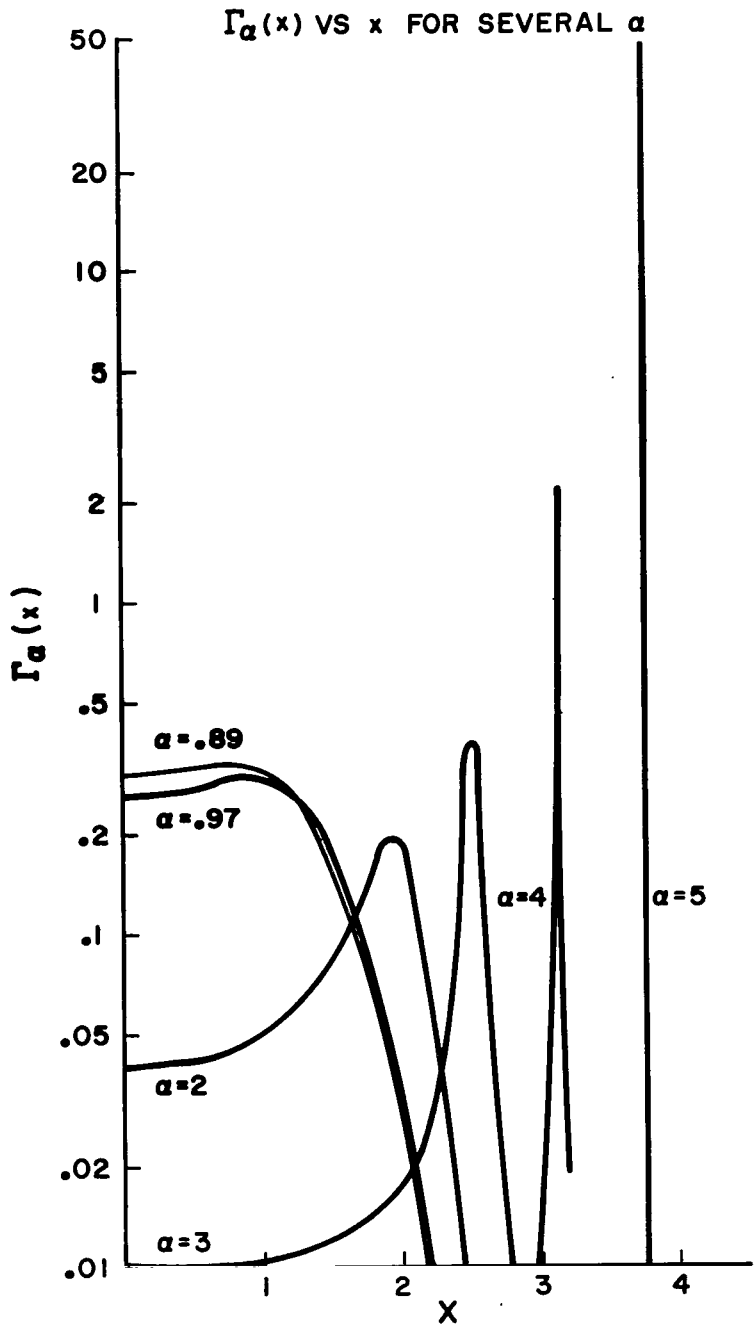

Figure 2.- The function $\exp(-x^2)\{[1 + \alpha^2 - \alpha^2 f(x)]^2 + \pi\alpha^4 x^2 \exp(-2x^2)\}^{-1}$ vs x.

Next, expressions for the maximum value Γ_{max} and the breadth of the maximum between points half as high as the maximum are easily derived:

$$\Gamma_{max} = \frac{2e^{(\alpha^2 + 3)/2}}{\pi\alpha^4(\alpha^2 + 3)} , \tag{17}$$

$$\frac{f_{1/2} - f_{-1/2}}{f_p} = \sqrt{2\pi}(\alpha^2 + 3)^2 e^{-(\alpha^2 + 3)/2} , \tag{18}$$

where $f_{1/2}$ and $f_{-1/2}$ are the frequencies of the points of the curve half as high as the maxima and f_p is the plasma frequency. From these expressions it is seen that the maximum becomes much larger, sharper, and narrower as α increases. We are, therefore, motivated to find the area under the curve, an easy matter:

$$\int_{-\infty}^{\infty} dx\ \Gamma_\alpha(x) \approx \frac{\sqrt{\pi}}{1 + \alpha^2} . \tag{19}$$

We now see that there is only a narrow range of the parameter α for which it is possible to both detect the existence of the maxima and to measure the shape of the satellite. For $\alpha \lesssim 1$ there is really no maximum at all. For really large α, which is the only case for which our approximate formulas are derived, the satellite has very little area. Since it will turn out that it is quite a problem to get the signal stronger than the noise, it is advisable to choose a small value of α. Accordingly, it seems that a value of 2 is appropriate, even though our approximate formulas are no longer accurate.

The fluctuation $\left\langle |Q_e(\omega)|^2 \right\rangle$ of Eq. (1) consists of two terms. For low atomic number and when the electron and ion temperatures are equal, β will be close to 1 for large α. In this case, a plot of the second term of Eq. (1) as a function of frequency consists of a rather flat plateau in the vicinity of the laser frequency that at $y_0 \approx 1.5$ decreases to zero gradually. Normally $\alpha \gg \beta$, and a plot of the first term consists of a very sharp, very high maximum. This maximum or satellite line is separated according to Eq. (16) by approximately the plasma frequency from

the laser frequency:

$$\omega \approx \omega_p \left[1 + \frac{3}{2\alpha^2}\right] , \tag{20}$$

if we remember that the above results relate to the density fluctuations of the plasma.

Because we are interested in the component of the total scattering resulting from that corresponding to either of the satellite lines, a comparison of the area under either satellite line and the area under the whole curve is desirable. The area under the satellite line is given by Eq. (19). From this relation we can deduce the area under the curve resulting from the second term of Eq. (1), by replacing α with β, and then expressing β in terms of α by means of Eq. (6). We find that:

$$Z\left(\frac{\alpha^2}{1+\alpha^2}\right)^2 \int_{-\infty}^{\infty} dy \; \Gamma_\beta(y) = \frac{\sqrt{\pi}\; Z\alpha^4}{\left(1+\alpha^2\right)\left(1+\alpha^2\left\{1+\frac{ZT}{T_i}\right\}\right)} , \tag{21}$$

$$\xrightarrow[\alpha\to\infty]{} \frac{\sqrt{\pi}\; Z}{1+\frac{ZT}{T_i}} . \tag{22}$$

The probability that in a scattering the scattering originates in the first term of Eq. (1) is then:

$$\frac{1+\alpha^2\left(1+\frac{ZT}{T_i}\right)}{1+\alpha^2\left(1+\frac{ZT}{T_i}\right)+Z\alpha^4} , \tag{23}$$

$$\xrightarrow[\alpha\to\infty]{} \frac{1+\frac{ZT}{T_i}}{Z\alpha^2} . \tag{24}$$

The results from the approximate formulas have been checked numerically for several values of α. These results are listed in Table I. It can be seen from this table that the agreement is superb between the numerical evaluations of Eq. (1) and the analytical approximations. From this table we also see that the

TABLE I

COMPARISON OF
ANALYTICAL APPROXIMATIONS AND NUMERICAL RESULTS

α	2	3	4	5
$\int_{-\infty}^{\infty} dx\ \Gamma_\alpha(x)$	.355	.175	.104	.0681
$\frac{\sqrt{\pi}}{1+\alpha^2}$	.355	.177	.104	.0682
$\left(\frac{\alpha^2}{1+\alpha^2}\right)^2 \int_{-\infty}^{\infty} dy\ \Gamma_\beta(y)$	.630	.755	.809	.835
$\frac{\sqrt{\pi}\ \alpha^4}{(1+\alpha^2)(1+2\alpha^2)}$	.630	.756	.809	.835
Value of x at which $\Gamma_\alpha(x)$ is maximum	1.95	2.50	3.13	3.76
$\sqrt{\frac{\alpha^2+3}{2}}$	1.87	2.45	3.08	3.74

relative probability of scattering in the line of interest to the total probability of scattering decreases with increasing α, but that the decrease is not especially serious.

The sum of the two terms in curly brackets in Eq. (1) is plotted in Figures 3 through 9. The fluctuation density itself has two peaks. One occurs very near the origin (the laser frequency) and is extremely sharp since:

$$y = \frac{\omega_p}{\omega_i} x = \sqrt{\frac{M}{m}}\, x >> x \quad . \tag{25}$$

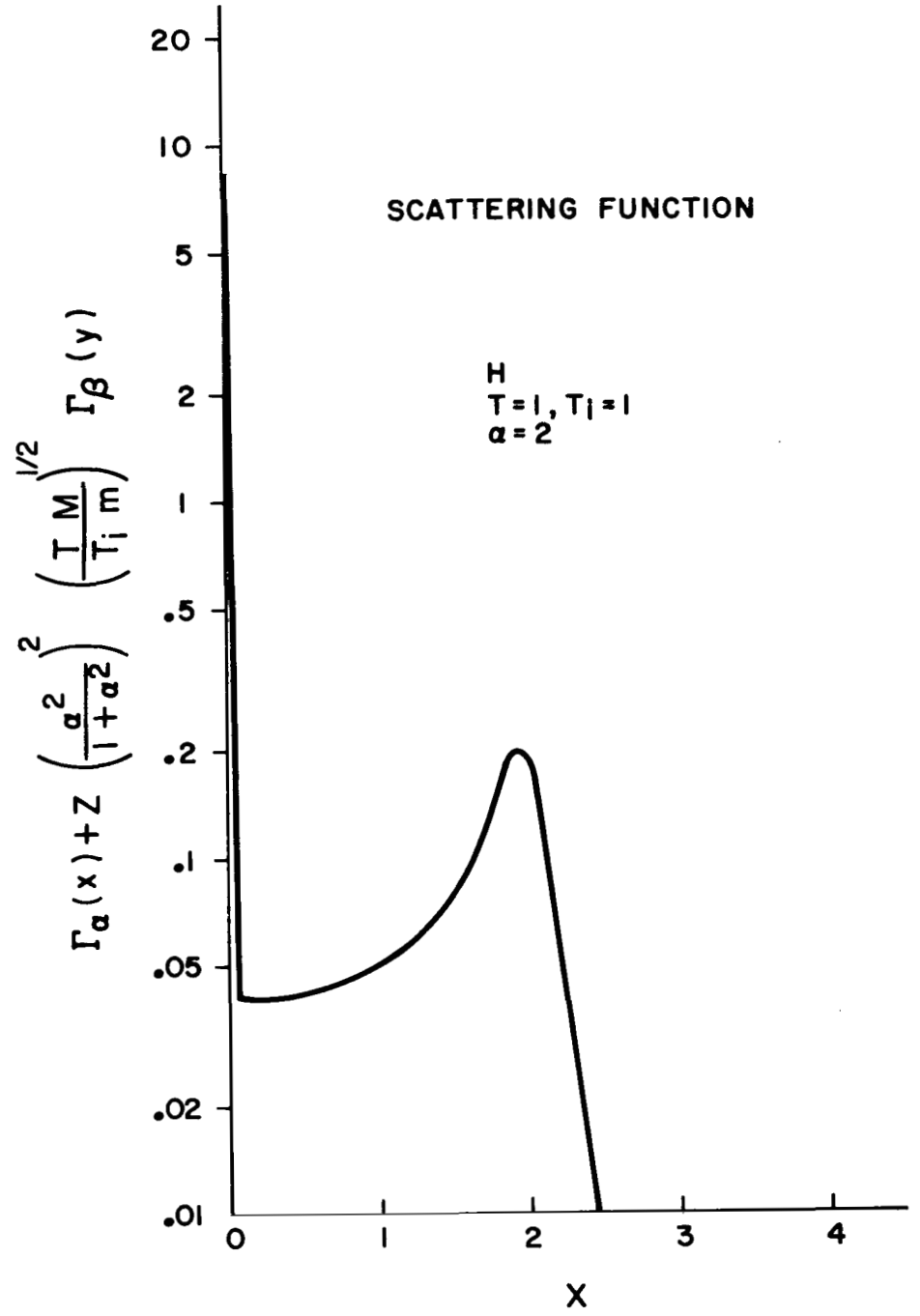

Figure 3.- A function proportional to the plasma charge density fluctuations vs normalized frequency for hydrogen at 1 eV electron and ion temperatures for $\alpha = 2$.

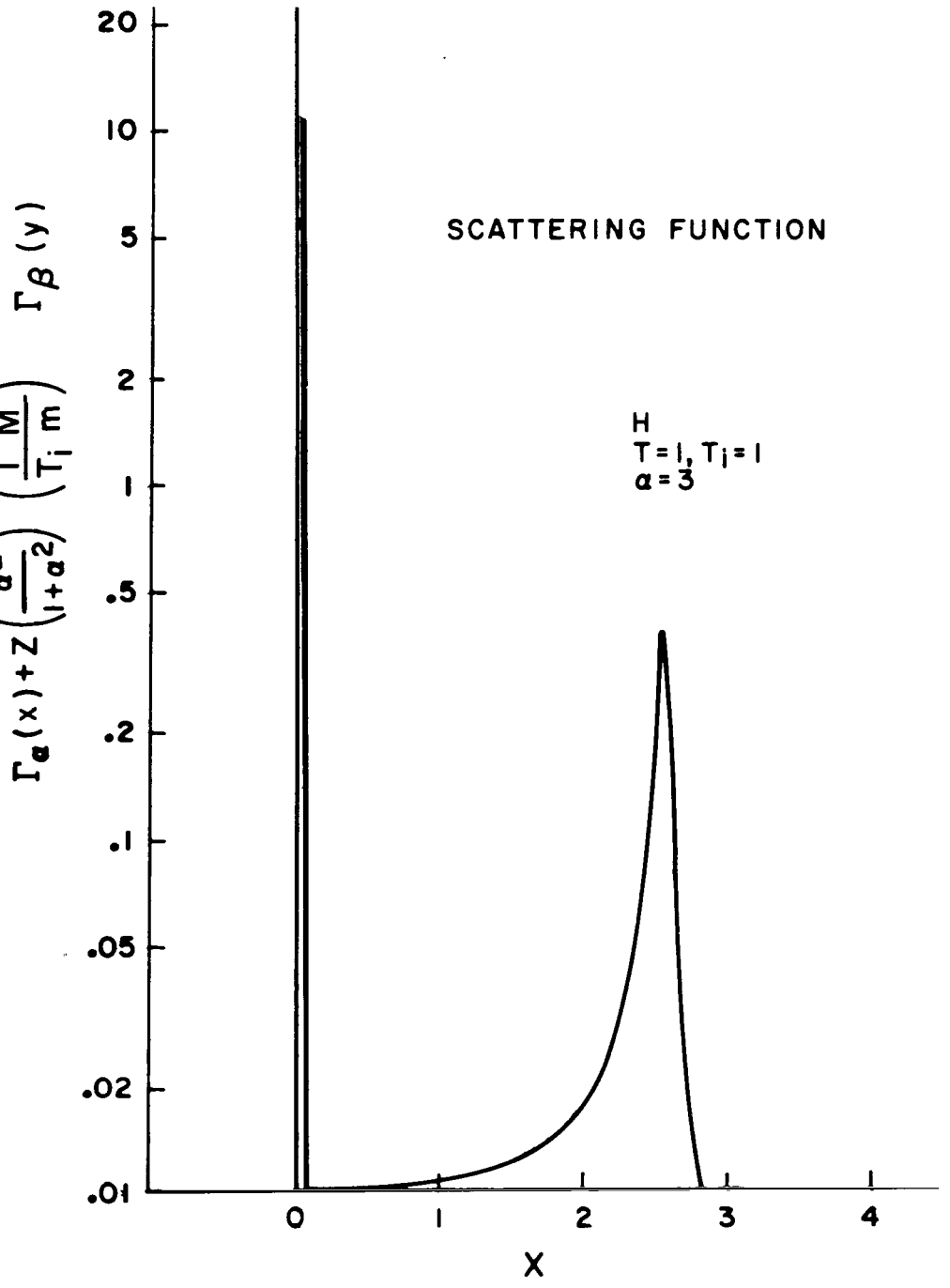

Figure 4.- A function proportional to the plasma charge density fluctuations vs normalized frequency for hydrogen at 1 eV electron and ion temperature for $\alpha = 3$.

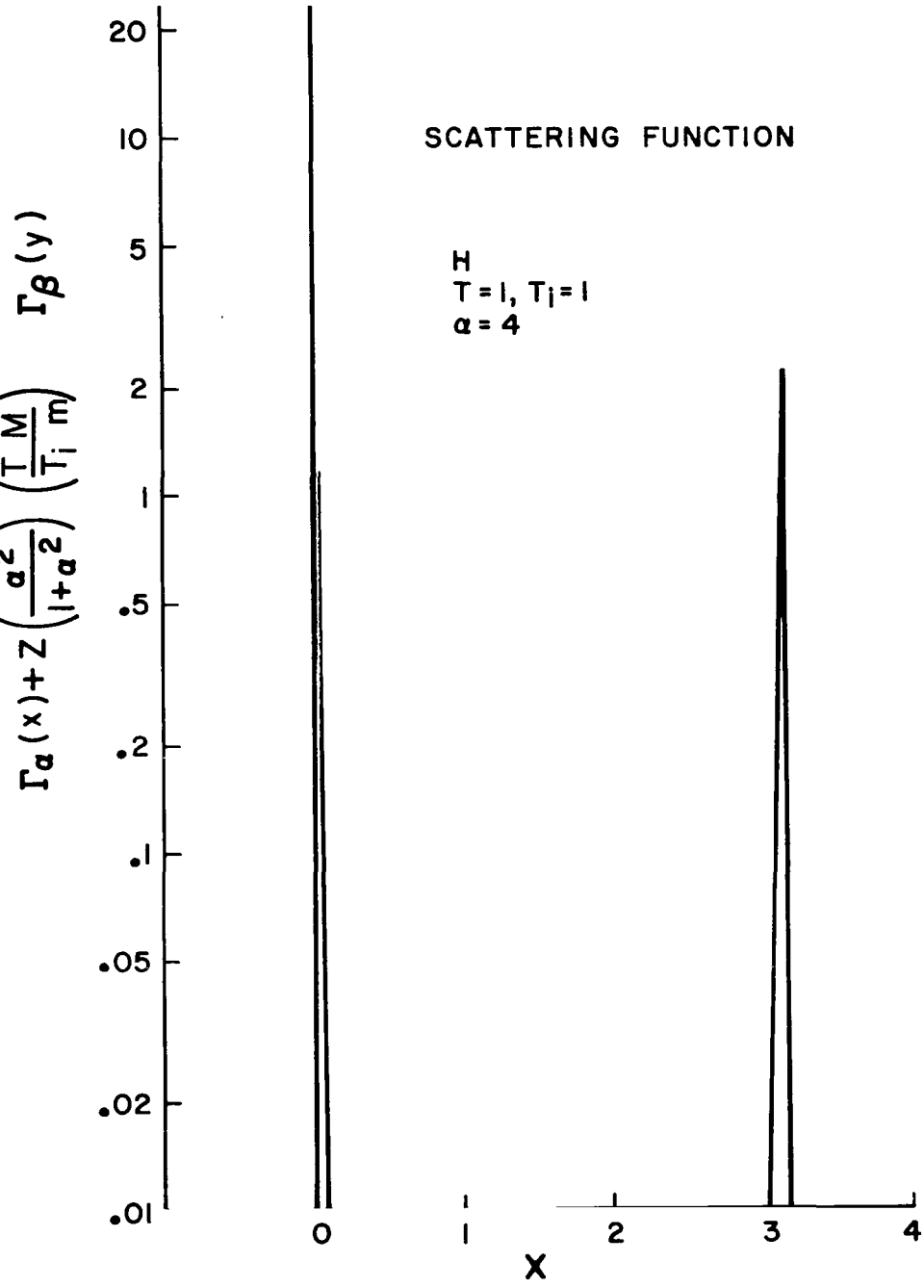

Figure 5.- A function proportional to the plasma charge density fluctuations vs normalized frequency for hydrogen at 1 eV electron and ion temperature for $\alpha = 4$.

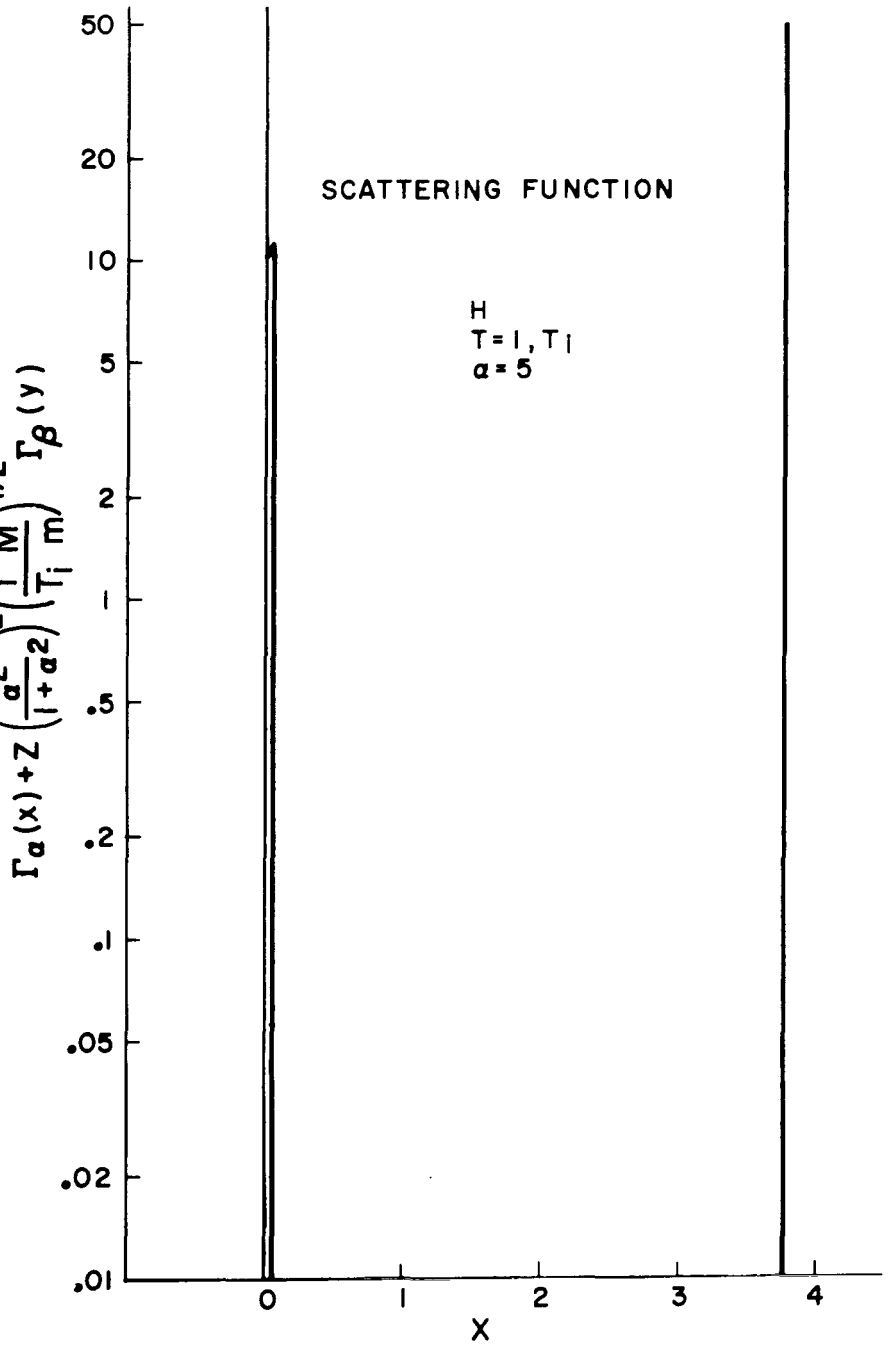

Figure 6.- A function proportional to the plasma charge density fluctuations vs normalized frequency for hydrogen at 1 eV electron and ion temperature for $\alpha = 5$.

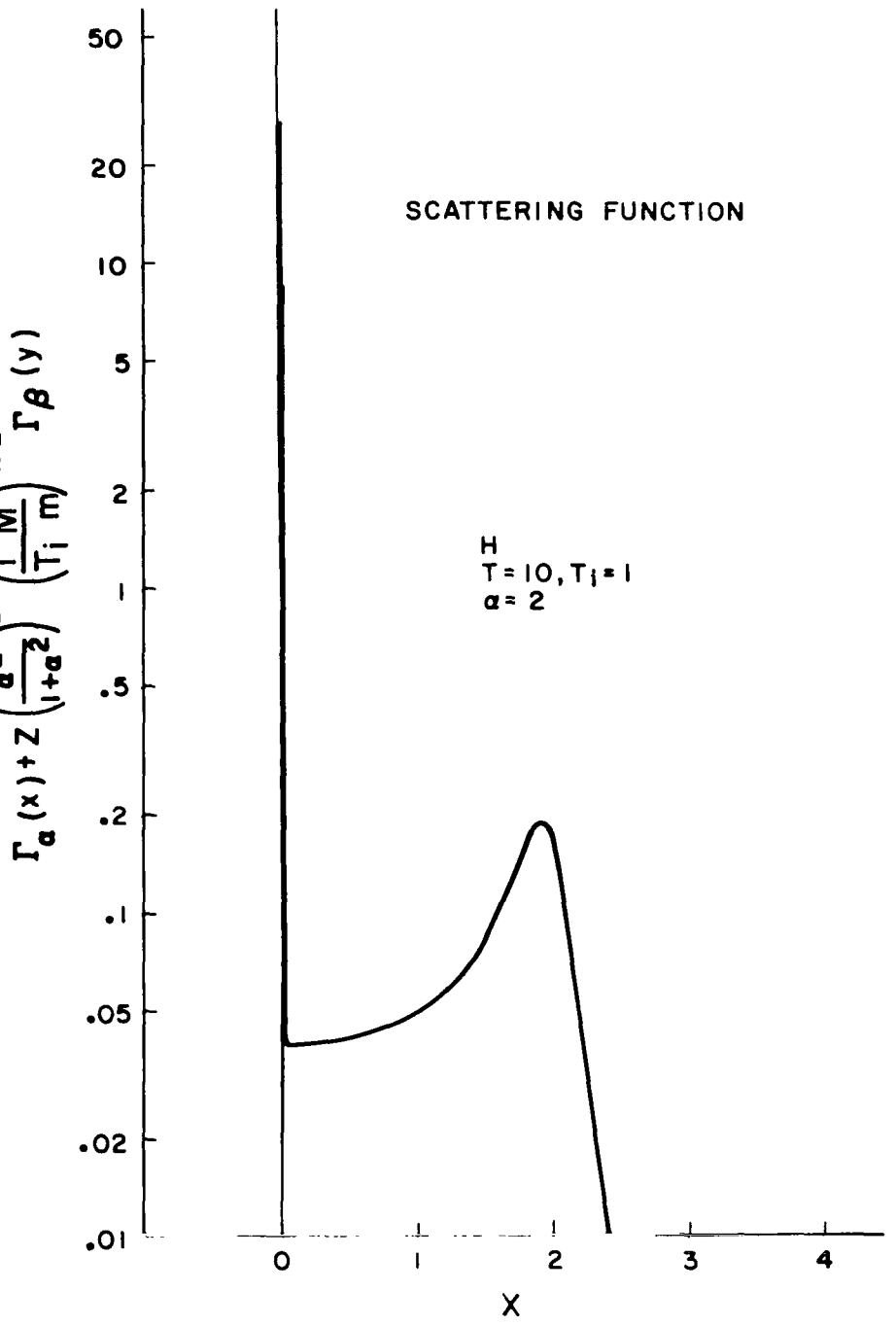

Figure 7.- A function proportional to the plasma charge density fluctuations vs normalized frequency for hydrogen at 10 eV electron and 1 eV ion temperature for $\alpha = 2$.

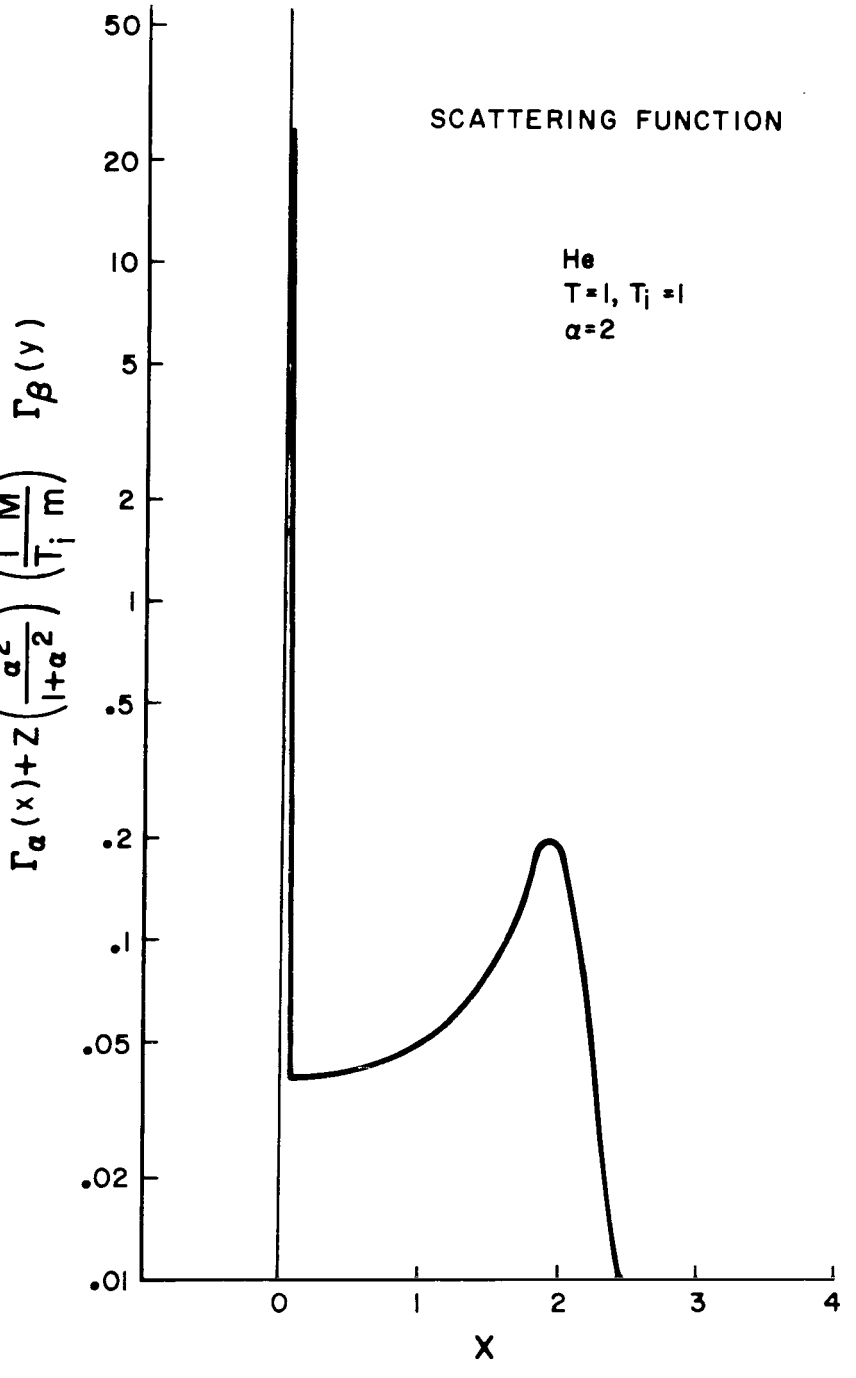

Figure 8.- A function proportional to the plasma charge density fluctuations vs normalized frequency for helium at 1 eV electron and ion temperature for $\alpha = 2$.

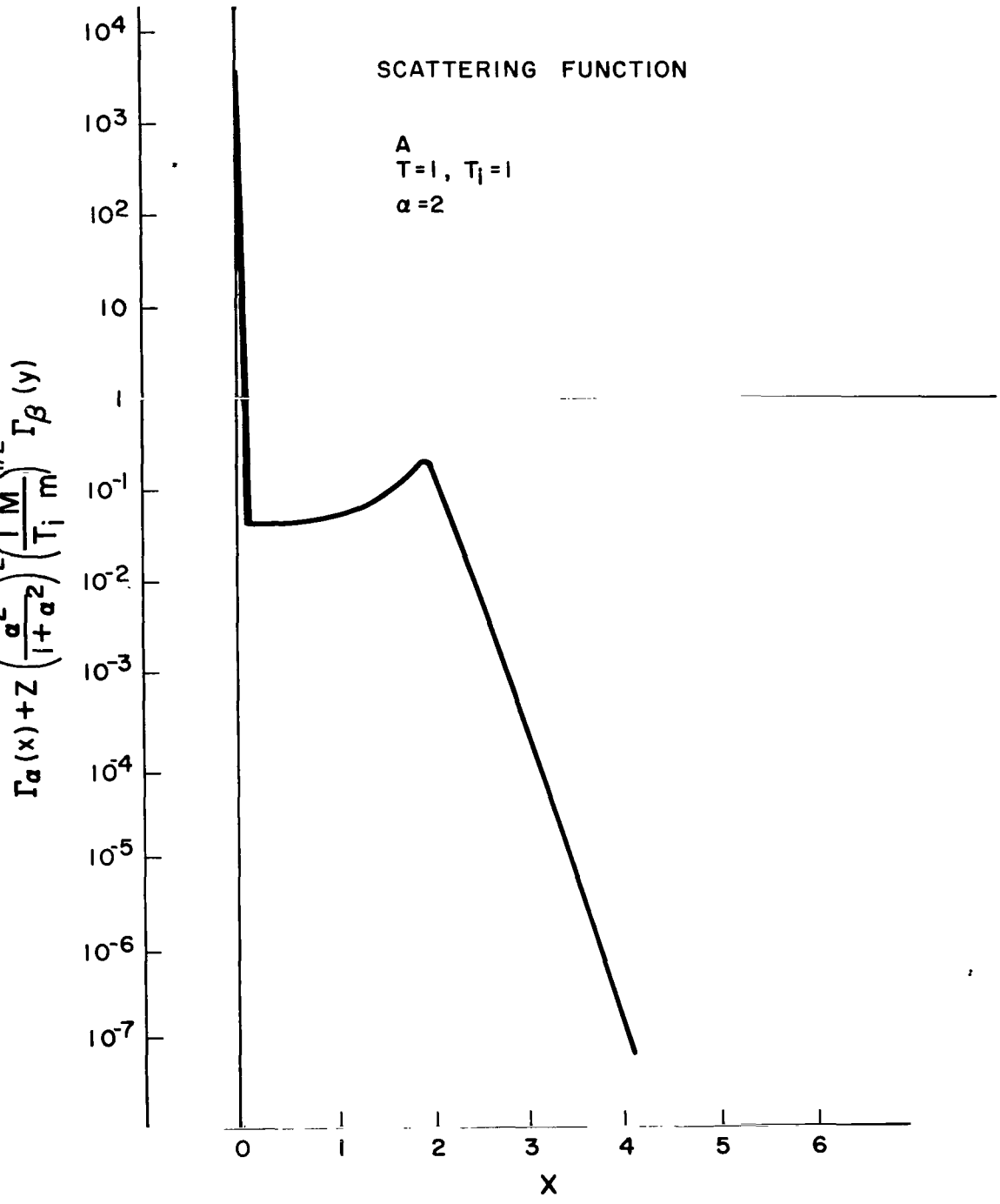

Figure 9.- A function proportional to the plasma charge density fluctuations vs normalized frequency for argon at 1 eV electron and ion temperature for $\alpha = 2$.

The other peak occurs some distance away from the origin and is neither high nor sharp for $\alpha \approx 1$. Of course, for $\alpha \gg 1$ this second peak may be very sharp and very high. The area under the curve decreases in accordance with Eq. (19). From these curves and approximate equations, it is easily seen that α is an all important parameter and that it must not be too large, for the probability of scattering resulting from the first term of Eq. (1) decreases fairly rapidly with increasing α, in accordance with Eq. (24). Again, α must not be too small either, for then no real maximum occurs, as may be seen from Figure 2. From these relationships it appears that the experiment can best be performed with a value for α of approximately 2. In any event, α must not be smaller than 1 nor larger than perhaps 4 if the shape of the satellite line is to be measured. Some representative cases for the probability of scattering caused by the first term of Eq. (1) are given in Table II. An electron temperature that is high relative to the ion temperature enhances this probability. From Table II it is also observed that increasing the atomic number decreases the probability of scattering in the line of interest only slightly. Thus, argon would be as good a gas to work with on this account as hydrogen, further argon arcs can be formed much more easily than hydrogen arcs. Of course, the results with hydrogen are much easier to interprete than those in argon because of the greater simplicity of the molecule.

TABLE II

PROBABILITY OF SCATTERING
FROM THE FIRST TERM OF EQ. (1)

α	Z	T/T_i	Probability
2	1	1	.36
3	1	1	.19
4	1	1	.11
5	1	1	.076
2	2	1	.29
	18	1	.21
2	1	10	.63

The angular plasma frequency ω_p is given by:

$$\omega_p = \sqrt{ne^2/m\varepsilon_0} \ . \tag{26}$$

RADIATION INTO DETECTOR

We must next compute the radiation that we expect to enter the detector after being scattered by the plasma. We shall find that a powerful laser and a very sensitive detector are needed.

Suppose there are n photons per unit volume. Since each photon travels at a speed c, nc of them will cross a unit area in a unit time. If there are N scattering centers per unit volume each of cross-section σ, there will then be $nc N\sigma$ interactions/ unit time-unit volume. If the beam has a cross-sectional area of A and if the length of the scattering medium is ℓ, then there are:

$$A\ell ncN \frac{d\sigma}{d\Omega} \tag{27}$$

photons scattered per unit time per unit solid angle.

If the laser source produces a beam of P watts at wavelength λ, the energy E of each photon is then given by:

$$E = hc/\lambda \ , \tag{28}$$

and there are

$$P\lambda/hc \tag{29}$$

photons produced per unit time, all of which stream through the area A. Thus, the photon flux is $P\lambda/hcA$, and the photon density is:

$$P\lambda/hc^2A \ . \tag{30}$$

The number of photons scattered per unit time per unit solid

angle is:

$$(\ell P\lambda/hc)N(d\sigma/d\Omega) \ , \tag{31}$$

and the power is given by:

$$\ell PN(d\sigma/d\Omega) \ . \tag{32}$$

Now, the differential cross-section for scattering unpolarized radiation is (ref. 1):

$$\frac{d\sigma}{d\Omega} = \frac{r_0^2}{2}\left(1 - \frac{1}{2}\sin^2\theta\right) \ , \tag{33}$$

where

$$r_0 = \mu e^2/4\pi m \ , \tag{34}$$

θ is the angle of scattering, and μ is the permeability. This includes scattering from both satellite lines and from the center line. We must multiply by the probability (23) that, in a scattering, the scattering takes place from one of the satellite lines. Thus, the differential scattering cross-section for scattering unpolarized radiation from the line of interest is:

$$\frac{d\sigma'}{d\Omega} = \left(\frac{r_0^2}{2}\right)\left(1 - \frac{\sin^2\theta}{2}\right)\left(\frac{1}{2}\right)\frac{\left[1 + \alpha^2\left(1 + \frac{ZT}{T_i}\right)\right]}{\left[1 + \alpha^2\left(1 + \frac{ZT}{T_i}\right) + Z\alpha^4\right]} \tag{35}$$

$$\approx \left(\frac{r_0^2}{4}\right)\left(1 - \frac{\sin^2\theta}{2}\right)\frac{\left(1 + \frac{ZT}{T_i}\right)}{Z\alpha^2} \ . \tag{36}$$

for large α. Thus, a small value of α gives the largest cross-section. As pointed out earlier, a value of $\alpha \lesssim 1$ produces no satellite at all, so we settle on a value of $\alpha = 2$ as about optimum.

The number of photons scattered per unit time and per unit solid angle is then

$$\frac{\ell P \lambda N}{hc} \frac{d\sigma}{d\Omega} = \frac{\ell P \lambda N r_0^2}{4hc} \left\{ 1 + \frac{Z\alpha^4}{1 + \alpha^2 \left[1 + \frac{ZT}{T_i} \right]} \right\}^{-1} \left\{ 1 - \frac{\sin^2 \theta}{2} \right\} . \quad (37)$$

We must next determine the solid angle subtended by the detector at the source. This angle will clearly be a function of the optical system between the detector and the source. Obviously, we want to collect as much of the signal as possible in order to get as high a signal-to-noise ratio as possible. This means that the optical system must be such that the scattered radiation fills the entrance cone of the detector, and that the small volume in which the scattering takes place must be imaged on the detector. If the entrance cone is not filled, then, clearly, the noise due to thermal radiation that gets into the detector can be reduced by stopping down this entrance cone with a refridgerated window.

The optical system will be assumed to be characterized by a focal length f, an object to system distance of u, and a system to image distance of v. It may consist of a lens or mirror. A mirror is preferable to a lens in that the mirror is subject to fewer aberrations than the lens. It seems possible to build a better mirror at 10.6μ than a lens; although, it is admitted that a lens can be used in situations where a mirror cannot. In either case, the various lengths are related by (ref. 3):

$$\frac{1}{u} + \frac{1}{v} = \frac{1}{f} . \quad (38)$$

The angles θ and ϕ of corresponding light cones at the scattering center and the detector, respectively are related by (ref. 3):

$$u \tan \theta = v \tan \phi . \quad (39)$$

Finally, the solid angle into which radiation may be scattered and get into the detector is given by

$$2\pi \left\{ 1 - \left[1 + \left(\frac{v}{u} \right)^2 \tan^2 \phi \right]^{-1/2} \right\} . \quad (40)$$

But, now, the detector to source area ratio B/A is related to u/v by

$$\frac{u}{v} = \frac{A}{B} \ , \tag{41}$$

so that the solid angle subtended at the scattering center by the entrance aperature of the optical system is given by:

$$2\pi\left\{1 - \left[1 + \frac{B}{A}\tan^2\phi\right]^{-1/2}\right\} . \tag{42}$$

We see that a figure of merit for the detector is given by:

$$B\tan^2\phi \approx B\phi^2 \ . \tag{43}$$

Because of the workings of an optical system, we see that the smaller the area of the scattering center, the larger the solid angle. Effectively, then, the optical system greatly increases the solid angle of the detector at the scattering center.

The power incident on the detector is, thus:

$$\frac{\pi\ell PNr_0^2}{2}\left\{1 + \frac{Z\alpha^4}{1+\alpha^2\left[1+\frac{ZT}{T_i}\right]}\right\}^{-1}\left\{1 - \frac{\sin^2\theta}{2}\right\}\left\{1 - \left[1 + \frac{B}{A}\tan^2\phi\right]^{-1/2}\right\} . \tag{44}$$

We must next work out the size of the scattering volume. Now, the radiation from the source, a laser, will be rather parallel. This radiation will be condensed by an optical system of some sort into a generally rhombehedron-of-revolution scattering volume within the plasma, as shown in Figure 10. The definitions of various quantities relating to the scattering volume are shown in Figure 11. From the relation (38), we learn that:

$$z = \frac{1}{\frac{1}{f} - \frac{1}{s}} \ , \tag{45}$$

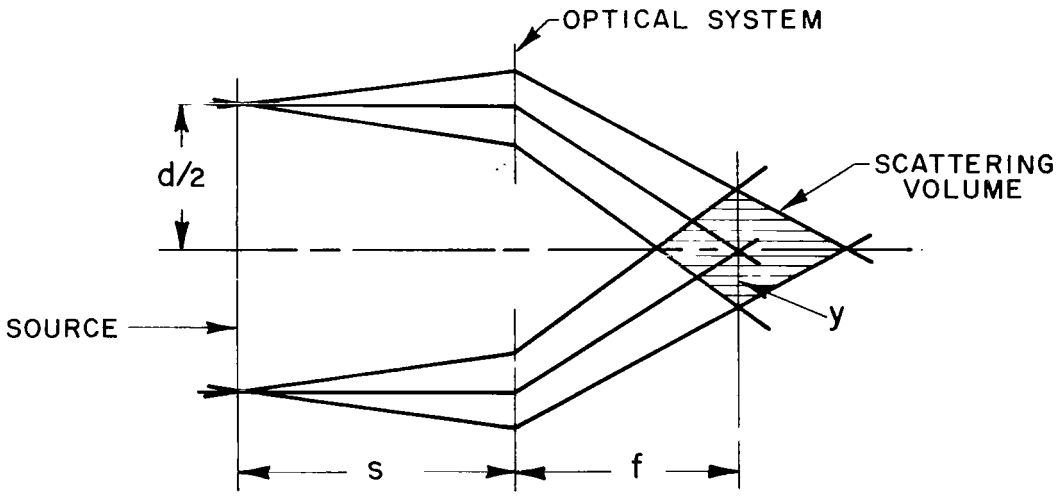

Figure 10.- Scattering volume in a plasma.

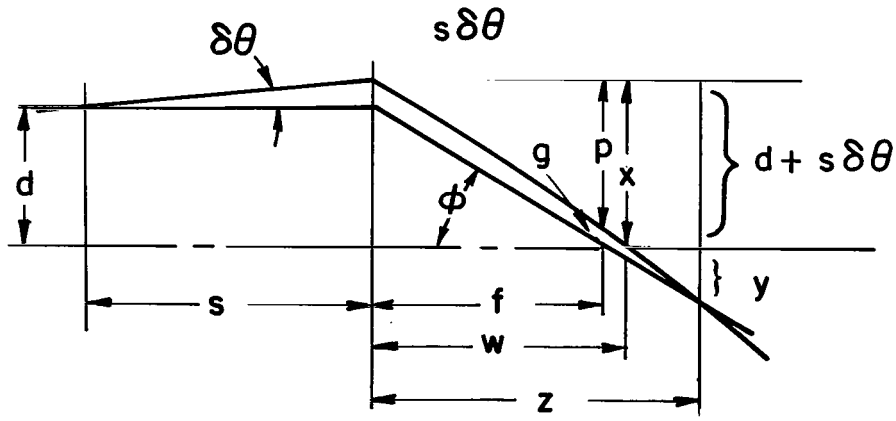

Figure 11.- Geometry relating to scattering volume.

and from the geometry we find that:

$$y = \frac{df}{s - f} , \tag{46}$$

therefore, that:

$$\frac{p}{y + d + s\delta\theta} = \frac{f(s - f)}{sf} , \tag{47}$$

so that:

$$p = d + (s - f)\ \delta\theta \tag{48}$$

and

$$g = d + s\delta\theta - p , \tag{49}$$

$$= f\delta\theta . \tag{50}$$

From Figure 11 we also see that:

$$\frac{w}{d + s\delta\theta} = \frac{sf}{(s - f)(y + d + s\delta\theta)} , \tag{51}$$

$$w = \frac{sf(d + s\delta\theta)}{sd + (s - f)s\delta\theta} . \tag{52}$$

The half-height of the rhombehedron of revolution is given by:

$$w - f = \frac{f^2\delta\theta}{d + (s - f)\delta\theta} . \tag{53}$$

The volume of the rhombehedron of revolution is:

$$\frac{2\pi}{3} \frac{[f\delta\theta]^3}{\left[\frac{d}{f} + \left(\frac{s}{f} - 1\right)\delta\theta\right]} , \tag{54}$$

and the area of the scattering rhombehedron projected on a plane parallel to the axis is then:

$$\frac{2[f\delta\theta]^2}{\left[\frac{d}{f} + \left(\frac{s}{f} - 1\right)\delta\theta\right]} . \tag{55}$$

Enormous attenuation is needed of the radiation between the laser and the detector. For this reason, it is insufficient to provide merely geometrical shielding; the radiation can still be scattered many times and get into the detector. Accordingly, the laser and plasma will be modulated at different frequencies. An electrical filter will be inserted in the output of the detector at a frequency equal to the sum of the modulation frequencies. The laser radiation may thus be heavily discriminated against. The detector is a square-law device, in that, its output current is proportional to the energy incident on it, i.e., to the square of the electric intensity of the incident radiation.

The theory for this process is almost trivial. The electric intensity $\mathscr{E}$ of the radiation from the laser has the form

$$\mathscr{E} = a_1[1 + a_2 \cos (2\pi f_a t)] \cos (2\pi f_\ell t) , \tag{56}$$

where a_1 and a_2 are constants, f_a and f_ℓ are, respectively, the frequencies of modulation and of the radiation. The plasma density n is modulated at a second audio rate f_b

$$n = b_1 + b_2 \cos (2\pi f_b t) . \tag{57}$$

The electric intensity $\mathscr{E}_s$ of the radiation scattered into the detector is proportional to the electric intensity of the radiation incident on the plasma and the density of the plasma:

$$\mathscr{E}_s = c_1 a_1 b_1 [1 + b_2 \cos (2\pi f_b t)] \cos 2\pi f_\ell t$$

$$\cdot [1 + a_2 \cos (2\pi f_a t)] . \tag{58}$$

Now the output current from the photodetector is proportional to the number of photons incident on it, i.e., to $\mathscr{E}_s^2$. Thus, there

will be the following frequencies present in the output:

$$0,\ f_b,\ 2f_b,\ f_a,\ f_a \pm f_b,\ f_a \pm 2f_b,\ 2f_b,\ 2f_a \pm f_b,\ 2f_a \pm 2f_b\ .$$

Of these, the most intense components occur at frequencies f_b and f_a. The next most intense occur at frequencies $f_a + f_b$ and $f_a - f_b$. For this reason, the components at $f_a + f_b$ or $f_a - f_b$ are selected, for it clearly does no good to select the components at either f_b or f_a.

The radiation from a CO_2 laser can be modulated in two ways: (1) the current passing through the laser may be modulated, and (2) the light output from the laser can be modulated. It is quite expensive to modulate the current passing through the laser; further, the degree of modulation in the middle audio range is limited because of the long life of one of the states in the CO_2 laser. Indeed, modulation much above 1 kHz is not practical. Electro-optical modulators for 10.6μ are still in the developmental stage. It would require a special, noncommercially-available wheel to modulate the radiation from the laser sinusoidally. However, the radiation from the laser can be chopped very easily up to a maximum frequency of about 1.5 kHz. We would, therefore, like to know the amplitude of the fundamental component in the chopped signal. From elementary Fourier analysis, this amplitude can be seen to be given by:

$$\frac{2}{T}\int_{T/2}^{T} dt\ \sin\left(\frac{2\pi mt}{T}\right) = \frac{(-)^m - 1}{\pi m} \tag{59}$$

for the signal shown in Figure 12. Thus, we may expect approximately 64 percent of the laser power to be in the fundamental component.

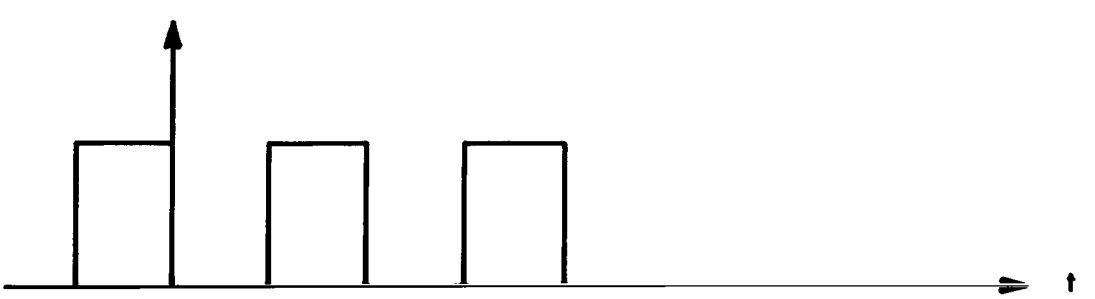

Figure 12. Chopped waveform.

Germanium doped with either mercury or copper forms a very sensitive detector at 10.6μ (ref. 4). These detectors must be cooled to liquid helium temperatures. A 2N3089A field-effect transistor in the source-follower mode provides a low-noise first-stage input to a low-noise amplifier. A 1- or 2-M resistor may be used between gate and ground and a 15-K resistor in the source lead. To reduce noise, these resistors and the FET are mounted on the liquid He dewar beside the Ge(Hg) or Ge(Cu) detector.

LIGHT SOURCE

The light source must be very bright in order to overcome various sources of noise in the system, should preferably create radiation at a single wavelength, and should provide highly collimated light that can be focussed to a fine point. A CO_2 laser is a suitable source for this application and can be made to meet the requirements. CO_2 lasers can produce 200 watts continuously in a single transition. The line width is more than sufficiently narrow for the experiment, since it is only 75 MHz wide (2.8×10^{-11} m).

The design of a laser is quite straightforward from Whitehouse's prescriptions (ref. 5). A CO_2 laser can produce approximagely 60 watts per meter. Since 200 watts is desired and since at least a 30 percent safety factor is desirable, the pipe must be 4.3 meters long. Therefore, we may as well make the pipe 15 ft long. From Figure 7 of Whitehouse, we learn that the tube diameter should be about 1 1/2 in. From Figure 4 of Whitehouse, we might expect a 4.2 kV/m drop in the discharge. Thus, a 25-keV supply is needed; to be safe and to provide flexibility a 30-keV supply is specified. A current of 100 mA seems appropriate according to Whitehouse's Figure 4. From his Figure 5, it is seen that such a current is approximately correct for maximum power output. The gas mixture should then be approximately correct for maximum power output. The gas mixture should then be approximately 0.6 torr of CO_2, 1.5 torr of N_2, and 6.0 torr of He and flow at a rate of 15 ft^3/min. From our Figure 13, a port is provided at each end; one to let the gas in, the other to let it out.

The end caps perform many functions for the laser, as follows.

(1) Support for the center tube.

(2) Provide a means for getting gas into the system.

(3) Provide electrodes for the gas discharge.

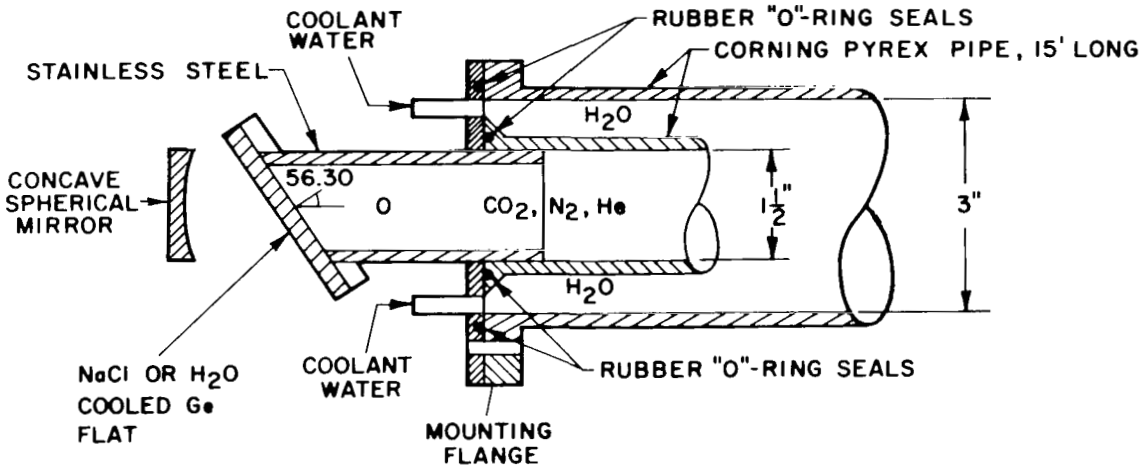

Figure 13.- End of CO_2 laser.

* * * * * *

(4) Hold the windows at the Brewster angle.

(5) Seal the tube gas tight.

(6) Hold the outer tube concentric with the inner tube.

(7) Provide inlets and outlets for the cooling water that flows between the two tubes.

(8) Hold the whole apparatus together.

To this end, the outer tube is forced tightly against the end plates by mounting flanges. Rubber O-rings are used to make the joints gas tight. The flanges bolted to the end cap and the other pipe thus form a rigid structure that carries the inner pipe concentrically.

The Brewster angle, $\overline{\phi}$, for the end windows is given by (ref. 6):

$$n = \tan \overline{\phi} \ , \tag{60}$$

where n is the index of refraction. Since the index of refraction for NaCl is about 1.5 at 10.6μ, the Brewster angle (between normal to the flat and the ray of radiation) is 56.32 deg. The thickness of the NaCl window is determined by the requirement that it withstand 1 atmosphere across the face of the inner pipe

cut at the Brewster angle. Unfortunately, the strength of NaCl seems to be not readily available. It is believed a quarter inch should be sufficient.

A mirror must be provided at each end of the pipe. One of these must be partially reflecting to let part of the radiation pass through. This mirror may conveniently consist of Ge. Since the index of refraction of Ge is 4, the fraction of the incident light that is reflected is (ref. 7):

$$\left(\frac{n - 1}{n + 1}\right)^2 = 0.36 \ . \qquad (61)$$

The other mirror may be a good reflector.

In order to increase the alignment tolerance, one of the two mirrors should be spherical (ref. 8). The focal point of this mirror should be beyond the flat mirror at the other end. Thus, the radius of curvature is great, being approximately 32 feet. The axis of this mirror should coincide with that of the tube to better than 10 percent of the (inner) tube diameter. Evaporated or electroplated gold provide a good reflecting surface for radiation at 10.6μ.

The CO_2 laser can oscillate in many modes. The mode selected will depend on laser gain and the distance between the mirrors. The laser may be forced to operate in only one transition by means of a very frequency selective end-mirror. This mirror, then, heavily discriminates against all other frequencies and, thus, reduces their gain enormously. There are several ways of constructing such a mirror. The easiest and least efficient consists in using a reflection grating. These are now commercially available, designed specifically for this purpose. The next simplest and least efficient method consists in using a prism with a suitable mirror. Finally, the most expensive and efficient method consists in using a (commercially available) Michelson interferometer for this purpose.

Even if a frequency selective end mirror can be used, the power produced in the single transition line can vary enormously as the distance between the mirrors changes. These changes may be caused by thermal expansion or vibrations due to acoustic noise. The effects of these changes can be minimized by a photodetector and piezoelectric-crystal mount for one of the mirrors. The photodetector monitors the output of the laser. As soon as this output decreases from the maximum, as a result of changes in mirror spacing, the signal from the photodetector decreases and changes the potential across the piezoelectric crystal, thereby

causing the mirror mounted on this crystal to move so that the distance between the two mirrors is restored to that giving maximum gain and power out. Such a system is commercially available.

The changes in distance between the mirrors can be reduced greatly by acoustic isolation, which is difficult, awkward, and expensive, and either by spacing the mirrors apart with low-expansion materials or by using a temperature-compensated mounting. A temperature-compensated mounting would consist of long rods made of a material having a low-expansion coefficient, such as invar, joined to short rods at one end having a higher expansion coefficient and going in the direction opposite to that of the long rods. The idea is to make the expansion of the short and long rods equal and opposite for a change of temperature, so that the unjoined ends of the long and short rods do not move with respect to each other as the temperature changes.

Cervit and superinvar are new materials having exceptionally low coefficients of thermal expansion (ref. 9). A few properties of Cervit are listed in Table III.

TABLE III

PROPERTIES OF CERVIT

Coefficient of thermal expansion 0°C to 50°C 25°C	 2×10^{-8}/°C ≈ 0/°C
Young's Modulus	1.3×10^{7} psi
Rigidity Modulus	5.5×10^{6} psi
Bulk Modulus	9.0×10^{6} psi
Density	2.5 g/cm^3

A second approach to high power in a single line exists. A short laser operating just above threshold can oscillate in only one transition. It can be stabilized by Cervit or superinvar. The low power produced by this laser can be greatly amplified by a long laser whose regenerative feedback has been reduced below the point at which the laser oscillates on its own.

The laser must be water cooled. The water used for cooling the laser must have a high resistivity to prevent bypassing the current through the discharge. The resistivity of tap water is not nearly high enough. The water used to cool the laser, therefore, must be demineralized, and the demineralized water must be pumped through a small heat exchanger. Tap water can be used to cool the other side of the heat exchanger. The plumbing must consist of stainless steel, Sn, glass, plastic (polyvinyl chloride pipes are commercially available), or other corrosion resistant material, so that ions will not be produced in the water and, thus, reduce the resistivity. Plastic piping and stainless steel pumps are commercially available and are suitable for this application. A 200-watt laser requires about 2000 watts of power. This energy must be removed as heat. The heat exchanger must process a relatively small amount of heat, viz., about 7000 Btu/hr. At a water flow rate of 5 gal/min, the water will rise about 1.5°C between inlet and outlet. This temperature rise is sufficiently low. Stainless steel heat exchangers are available commercially.

THERMAL NOISE

We must calculate the signal-to-noise ratio of our system. There are two sources of noise we must consider, (1) bremsstrahlung from the plasma, and (2) thermal noise from the objects seen by the detector. Bremsstrahlung noise will be discussed in the next section.

Thermal noise originates from the following sources:

(1) The cold walls of the dewar surrounding the detector. This source of noise is completely negligible.

(2) The part of the optical system seen by the source. This component must also be negligible if it is assumed the optical elements absorb no radiation, unless other elements are specially cooled.

(3) The plasma. This is very far from thermal equilibrium and is so sparse that we neglect, therefore, the thermal radiation from this source.

(4) The wall of the plasma container. If this wall is perfectly black, it is easy to compute the radiation emitted by it. If the wall is perfectly reflecting, then we must consider the radiation from the objects seen by the detector through the back wall of the plasma-confining cylinder. It is also clear that the thermal noise could be reduced considerably by cooling the area seen by the detector. To this end, a cylinder with an axis parallel to the direction of viewing is

affixed to the plasma-confining cylinder. The first cylinder is of a large enough diameter that the detector sees only the end of the cylinder. The cylinder is cooled to a low temperature so that very little thermal noise is radiated into the detector.

We must next estimate the thermal noise power getting into the detector. This calculation can be conveniently subdivided into the following steps.

(1) A computation of the area of the cylinder seen by the detector.

(2) A calculation of the flux of thermal radiation getting into the detector from the brightness of the wall seen by the detector.

(3) A calculation of the brightness of the wall from its temperature.

(4) A computation of the thermal noise power flowing into the detector from the thermal power getting into the detector.

Only the fluctuations in the radiation getting into the detector correspond to noise. A steady, nonfluctuating flow of thermal radiation into the detector is not, per se, noise, for, in principle, the steady current resulting from this radiation could be cancelled out. To reduce the fluctuations (absolute, not fractional) in this steady current of photons (or electrons in the external circuit), a very narrow bandpass optical filter is inserted just before the detector. This filter greatly reduces the current of photons into the detector and, thus, the absolute fluctuations in this current.

The simple system shown in Figure 14 is assumed. The optical system might consist of a Cassegrainian mirror arrangement. The distance of the image of the sector of the cylinder seen by the detector from that detector is given by an expression of the form (ref. 3):

$$\frac{1}{\ell} = \frac{1}{f} - \frac{1}{d + u} \quad . \tag{62}$$

Therefore, the area of the cylinder seen by the detector is:

$$\pi (v - \ell)^2 \tan^2 \phi \quad . \tag{63}$$

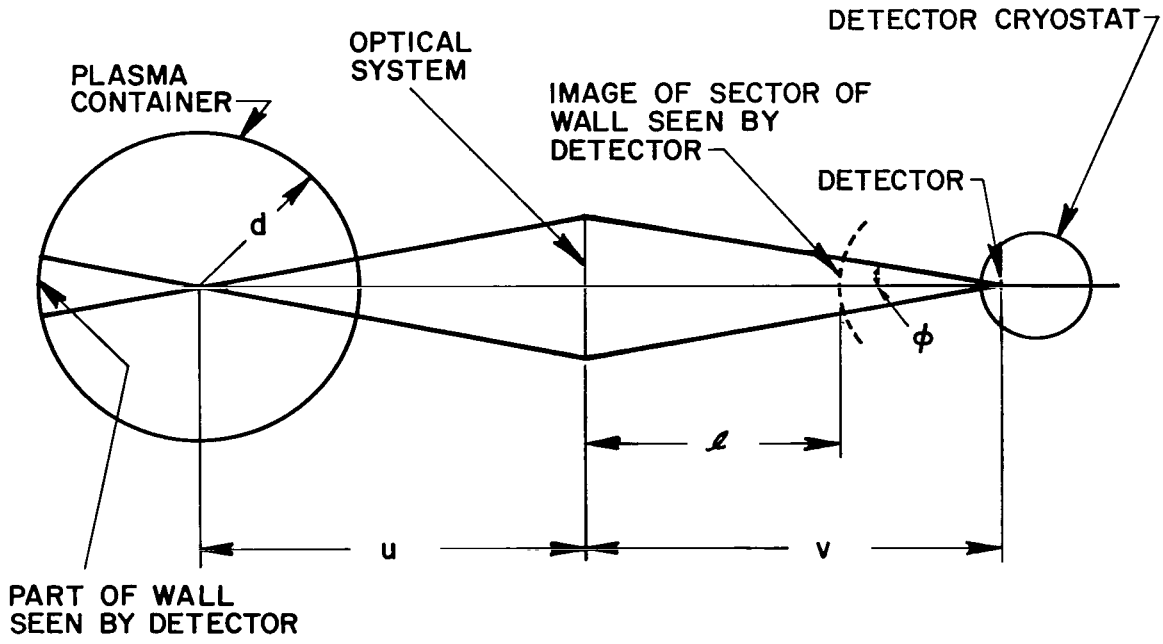

Figure 14.- Detector optical system.

* * * * * *

Now, the absorption of the optical system is negligible if properly designed. Therefore, the brightness of the image is the same as that of the wall seen by the detector. The solid angle of the detector at the image of the cylinder is:

$$\frac{B}{(v - \ell)^2} , \tag{64}$$

where B is the area of the detector. Therefore, the radiation getting into the photodetector from the image is (ref. 6):

$$\pi \mathscr{B} B \tan^2 \phi , \tag{65}$$

where $\mathscr{B}$ is the brightness of the wall. Note that the distance of the detector from the optical system has cancelled out. The only variables that are significant are the solid angle of the detector and the detector area. The smaller the detector area the less the noise. Note that we have assumed that the detector container forms the aperture stop of the system.

We must next work out the brightness of a black body source of radiation. The flux of radiation F_ν (power per unit area per unit frequency ν) radiated from a black body is given by (refs. 10, 11):

$$F_\nu = \frac{2\pi h}{c^2} \frac{\nu^3}{e^{(h\nu/\kappa T)} - 1} , \tag{66}$$

where κ is Boltzmann's constant, T is the absolute temperature of the wall, and h is Planck's constant. The brightness of many objects obeys Lambert's law, according to which the brightness of the object is independent of the angle of observation. Under these circumstances, the brightness $\mathscr{B}$ of the wall is approximately (ref. 12):

$$\mathscr{B} = \frac{2h}{c^2} \frac{\nu^3 \cos\theta}{e^{(h\nu/\kappa T)} - 1} , \tag{67}$$

where θ is the angle between the normal to the surface and the angle of observation.

The fluctuation in energy for photons from some source may be derived from the grand canonical ensemble or from the canonical ensemble. The fraction f_j of all ensembles in the state j is given by (ref. 10):

$$f_i = \frac{e^{-E_i/\kappa T}}{Z} , \tag{68}$$

where Z is the partition function for the canonical ensemble and is given by

$$Z = \sum_j e^{-E_j/\kappa T} , \tag{69}$$

where κ is Boltzmann's constant, T is the absolute temperature, and E_j is the energy of the j'th state. The mean of the energy E squared is then given by (ref. 13):

$$\overline{E^2} = \frac{\sum_j E_j^2 e^{-E_j/\kappa T}}{\sum_j e^{-E_j/\kappa T}} = \frac{1}{Z} \frac{\partial^2 Z}{\partial (1/\kappa T)^2} , \tag{70}$$

and the mean energy is given by:

$$\overline{E} = \frac{\sum_j E_j e^{-E_j/\kappa T}}{\sum_j e^{-E_j/\kappa T}} = \frac{1}{Z} \frac{\partial Z}{\partial (1/\kappa T)} . \tag{71}$$

Now

$$\frac{\partial \overline{E}}{\partial (1/\kappa T)} = \frac{1}{Z} \frac{\partial^2 Z}{\partial (1/\kappa T)^2} - \frac{1}{Z^2}\left[\frac{\partial Z}{\partial (1/\kappa T)}\right]^2 , \tag{72}$$

$$= \overline{E^2} - (E)^2 . \tag{73}$$

Again,

$$\frac{\partial \overline{E}}{\partial T} = \frac{1}{\kappa T^2} \frac{\partial \overline{E}}{\partial (1/\kappa T)} , \tag{74}$$

so that

$$\overline{E^2} - (\overline{E})^2 = \kappa T^2 \frac{\partial \overline{E}}{\partial T} . \tag{75}$$

According to Planck's formula, the mean energy of black body radiation contained in a volume ΔV between a frequency ν and $\nu + \Delta\nu$ is given by (refs. 10, 13):

$$nh\nu = \overline{E} = \frac{8\pi^2 h\nu^3 \, \Delta\nu\Delta V}{c^3\left[e^{(h\nu/\kappa T)} - 1\right]} . \tag{76}$$

Therefore,

$$\overline{E^2} - (\bar{E})^2 = \frac{8\pi^2 (h\nu)^2 \nu^2 \, \Delta\nu\Delta V \, e^{h\nu/\kappa T}}{c^3 \left[e^{h\nu/\kappa T} - 1\right]} , \tag{77}$$

$$= h\nu\bar{E} + \frac{c^3 \overline{E^2}}{8\pi^2 \nu^2 \, \Delta\nu\Delta V} . \tag{78}$$

The classical result for photons regarded as particles comprises the first term. The classical result for photons regarded as electromagnetic waves comprises the second term.

The fluctuation in the number of photons is given by (ref. 10):

$$\overline{n^2} - (\bar{n})^2 = \frac{\overline{E^2} - (\bar{E})^2}{(h\nu)^2} , \tag{79}$$

$$= \frac{n e^{h\nu/\kappa T}}{e^{h\nu/\kappa T} - 1} . \tag{80}$$

The present result can also be easily derived from the grand canonical ensemble. The probability of finding n_j particles in state j is given by

$$P(n_j) = \frac{e^{-(E_o + E_j) n_j/\kappa T}}{\sum_j e^{-(E_o + E_j) n_j/\kappa T}} . \tag{81}$$

It is easily seen that

$$\sum_{n_j=0}^{\infty} e^{-(E_o + E_j) n_j/\kappa T} n_j = \frac{e^{-(E_o + E_j) n_j/\kappa T}}{\left[1 - e^{-(E_o + E_j) n_j/\kappa T}\right]^2} , \tag{82}$$

$$\sum_{n_j=0}^{\infty} e^{-(E_o + E_j)n_j/\kappa T} n_j^2 = \frac{e^{-(E_o + E_j)n_j/\kappa T}}{\left[1 - e^{-(E_o + E_j)n_j/\kappa T}\right]^2} + 2 \frac{e^{-2(E_o + E_j)n_j/\kappa T}}{\left[1 - e^{-(E_o + E_j)n_j/\kappa T}\right]^3} , \quad (83)$$

therefore,

$$\bar{n}_j = \frac{1}{e^{-(E_o + E_j)n_j/\kappa T} - 1} , \quad (84)$$

$$\overline{n_j^2} = \frac{1}{e^{-(E_o + E_j)n_j/\kappa T} - 1} + \frac{2}{\left[e^{-(E_o + E_j)n_j/\kappa T} - 1\right]^2} , \quad (85)$$

so that

$$\overline{n_j^2} - (\bar{n}_j)^2 = \bar{n}_j\left[1 + (\bar{n}_j)\right] . \quad (86)$$

Because the number of photons need not be conserved, the constant E_o, which is normally determined by the number of particles in an Einstein-Bose system, may be taken to be 0 for convenience. The previous result now follows immediately.

Next, from the fluctuation in numbers of photons of particular energy, we must derive the noise that results. Because we would like to apply this result both to thermal radiation and bremsstrahlung, we would like to express our answer in terms of the flux F_ν per unit frequency at the frequency ν.

The fluctuation $\sqrt{\overline{\Delta E^2}}$ in the energy passing through an area A per unit time is given by Eq. (86) to be (ref. 11):

$$\sqrt{\overline{\Delta E^2}} = \{h\nu(1 + n)AF_\nu \Delta\nu\}^{1/2} . \quad (87)$$

From this expression we must determine the fluctuation in power. The simplest method of doing this is to recognize that we are

concerned here with the shot effect of photons and to establish a duality between this shot effect and that involving electrons. Now, for electrons of charge e that create an (average) electrical current of I_o, the fluctuation $\overline{q^2}$ in charge arriving at a terminal is given by (ref. 14):

$$\overline{q^2} = eI_o \ . \tag{88}$$

The mean square fluctuation $\overline{i^2}$ in the current is

$$\overline{i^2} = 2\Delta f e I_o \ , \tag{89}$$

where Δf is the bandwidth of the detector used to measure the fluctuation. As current is charge per unit time, and power is energy per unit time, the square of the noise power, i.e., the mean square fluctuation in power, due to the particulate character of photons is (ref. 11):

$$2\Delta f h\nu(1 + n)AF_\nu\Delta\nu \ . \tag{90}$$

The noise power $\sqrt{\overline{\Delta W_T^2}}$ for the photons of thermal radiation is then

$$\sqrt{\overline{\Delta W_T^2}} = \left\{\left[\frac{2h\nu^3 \cos\theta}{c^2(e^{h\nu/\kappa T} - 1)} \pi B \tan^2\phi\right]\cdot\left[2\Delta f h\nu\left(1 + \frac{1}{e^{h\nu/\kappa T} - 1}\right)\Delta\nu\right]\right\}^{1/2} , \tag{91}$$

$$= \frac{2\sqrt{\pi}[\Delta f B \cos\theta \ c\,\Delta\lambda]^{1/2} hc \tan\phi}{[\exp(hc/2\kappa T\lambda) - \exp(-hc/2\kappa T\lambda)]\lambda^3} \ . \tag{92}$$

The first factor in Eq. (91) represents the power due to thermal radiation that gets into the detector as deduced from Eqs. (65) and (67). The second factor represents the fluctuation in this

power that causes noise as given by expression (90). The thermal noise power into the detector is given by expression (92) then. Here, it must be kept in mind that $\Delta\nu$ is the bandwidth of the optical system centered at frequency ν, and Δf is the bandwidth of the electrical system following the detector. Because the optical bandwidth $\Delta\nu$ is very narrow compared with the optical frequency, there is no need to integrate over this optical bandwidth.

Indeed, to reduce the noise in the detector resulting from fluctuations in the photon flux streaming into the detector, a very narrow, bandpass optical filter will be inserted in this stream. To reduce thermal noise radiated from this optical filter, it will be mounted on the dewar and cooled to liquid helium temperatures. It is practical to make such an optical filter only 0.1μ wide centered at 10.59μ, the wavelength of the CO_2 laser. Further, the transparency of the filter in the passband will exceed .35. It is this filter that determines $\Delta\nu$ above. Δf is determined by the lock-in amplifier that has been mentioned earlier.

After some amplification by the low-noise amplifier, the signal is applied to the narrow, bandpass electrical filter to reject noise. This filter is centered at the sum frequency of the frequency at which the laser beam is chopped and the frequency at which the plasma is modulated.

The filter is effectively narrowed even further and even more discrimination against noise is provided by applying the output of the low-noise-amplifier-filter combination to a lock-in amplifier. The reference signal for this amplifier is provided by a single-sideband mixer. This mixer is excited by the chopper, and by the 60-Hz signal used to modulate the plasma. The detected signal is essentially heterodyned to zero frequency by the reference signal and is applied through a low-pass filter to the output meter.

The bandwidth of the low-pass filter determines the improvement in the signal-to-noise ratio achieved by the lock-in amplifier. If the signal-to-noise ratio at the output of the low-noise amplifier is referred to a 1 Hz bandpass, then the improvements that may be expected in the signal-to-noise ratio for various integration times as a result of the lock-in amplifier are shown in Table IV. The improvements in dB varies as 5 log t, where t is the integration time. Obviously, the increments of improvements by waiting longer and longer diminish rapidly.

TABLE IV

IMPROVEMENT IN SIGNAL-TO-NOISE RATIO
BY A LOCK-IN AMPLIFIER FOR VARIOUS INTEGRATION TIMES

Integration Times	Improvement in Signal-to-Noise Ratio (dB)
1 second	0.0
1 minute	8.9
1 hour	17.8
1 day	24.6
1 week	28.9
1 month	32.1
1 year	37.4
1 century	42.5

BREMSSTRAHLUNG NOISE

Although the thermal radiation from the plasma is considered to be negligible compared with the radiation from the container walls, we must consider the bremsstrahlung from the plasma. Here we encounter problems, for bremsstrahlung formulas are usually applied to photons of far greater energies than those of current interest. Nevertheless, we shall use the bremsstrahlung formula for our very low photon energies.

The number of photons emitted per unit volume per unit time per unit frequency is given by (refs. 15, 16):

$$d\mathcal{N} = \frac{16}{3}(hZ)^2\left(\frac{e^2}{2\varepsilon_o hc}\right)\left(\frac{e^2}{4\pi\varepsilon_o mc^2}\right)^2 mc^2\sqrt{\frac{2}{\pi m\kappa T}}$$

$$\cdot\ \frac{\exp -(h\nu/2\kappa T)}{h\nu/2\kappa T}\ K_o(h\nu/2\kappa T)\ d(h\nu/2\kappa T)\ . \qquad (93)$$

The photon power emitted per unit frequency per unit volume is

$$h\nu\ d\mathcal{N}. \qquad (94)$$

The volume of plasma contributing to the Bremsstrahlung is given by expression (54). The solid angle subtended by the entrance aperture of the detector at the plasma scattering volume is given by expression (42). This solid angle divided by 4π is the probability that a photon once scattered is scattered in the direction of the detector. Thus, the bremsstrahlung power scattered into the detector from the plasma is

$$h\nu\left\{\frac{\sqrt{2}}{6\pi^{5/2}}\ \frac{e^6 n^2 Z^2 K_0(hc/2\kappa T\lambda)\ \Delta\lambda e^{-(hc/2\kappa T\lambda)}}{\varepsilon_0^3 hm^{3/2}c^3(\kappa T)^{1/2}\lambda}\right\}$$

$$\left\{\frac{2\pi}{3}\ \frac{(f\delta\theta)^3}{\left[\frac{d}{f}+\left(\frac{s}{f}-1\right)\delta\theta\right]}\right\}\left\{\frac{2\pi}{4\pi}\left[1-\left(1+\frac{B}{A}\tan^2\phi\right)^{-1/2}\right]\right\}. \tag{95}$$

The noise resulting from the current of photons originating in the bremsstrahlung process is then found from this expression and from expression (90), and is finally

$$\left\{\frac{1}{9\pi}\sqrt{\frac{2}{\pi}}\ \frac{he^6 n^2 Z^2 \Delta f}{\varepsilon_0^3 c\ m^{3/2}}\ \frac{\Delta\lambda\left[1-\frac{1}{\sqrt{1+\frac{B}{A}\tan^2\phi}}\right][f\delta\theta]^3}{\lambda^3(\kappa T)^{1/2}\left[\frac{d}{f}+\left(\frac{s}{f}-1\right)\delta\theta\right]}\right.$$

$$\left.\frac{K_0(hc/2\kappa T\lambda)}{[e^{h\nu/2\kappa T}-e^{-h\nu/2\kappa T}]}\right\}^{1/2}. \tag{96}$$

The light scattered from the plasma must now compete with the thermal noise created by the wall and the bremsstrahlung from the plasma, and any noise specifically arising from the detector itself.

NUMERICAL RESULTS

The relations needed to compute signal-to-noise ratios have been all derived; it now remains to make sense from them. Accordingly, a parameter study has been carried out with a small

computer. In view of the large number of parameters, it is impractical to evaluate the various noise formulas for all possible combinations of sets of complete parameters. This problem is alleviated by computing and tabulating the results in small subgroups and by plotting the results.

In Figure 15, the area of a circular detector is plotted as a function of its radius.

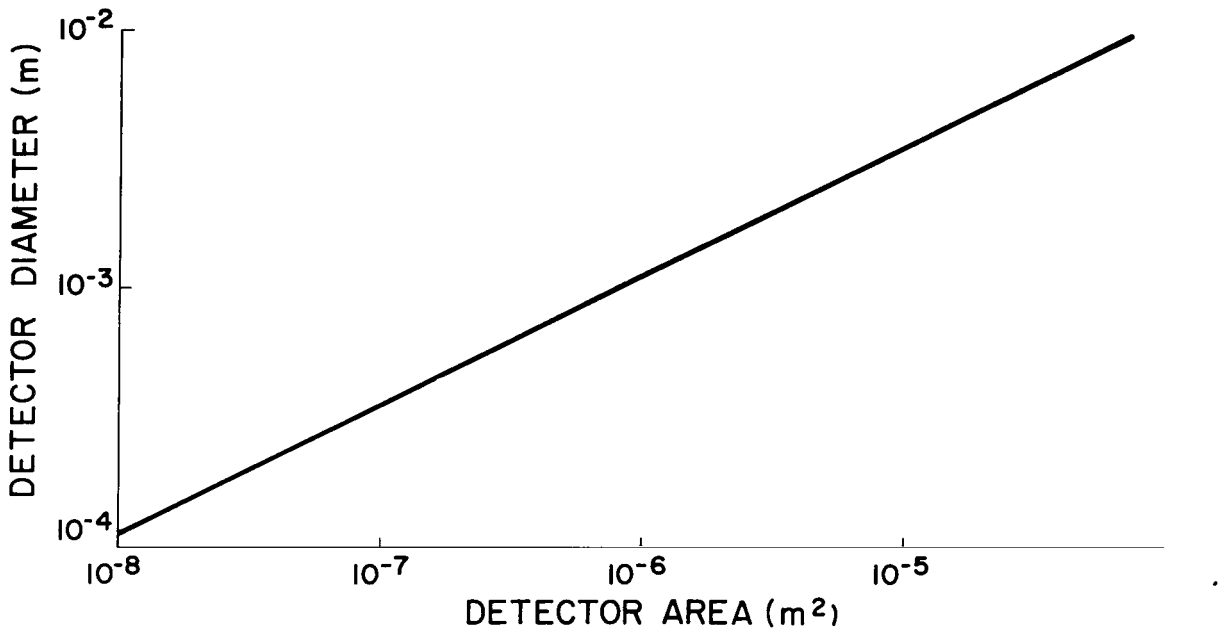

Figure 15.- Detector area vs detector diameter.

The area, irradiated by the laser and perpendicular to the optic axis, of the plasma radiating into the detector is plotted in Figure 16 in accord with Eq. (55), and as a function of the focal length of the optical system between the laser and plasma. This area is only very weakly dependent on the distance between the laser and the optical system between the laser and the plasma.

The solid angle subtended by the detector at the plasma is plotted in Figure 17, in accord with Eq. (42), as a function of the area of the source for various values of the detector area.

It will be remembered that a parameter called α is rather narrowly determined by the requirement that satellite lines exist and that they be of sufficient width that this width be resolvable. The angle of scattering (θ) is really determined by combining

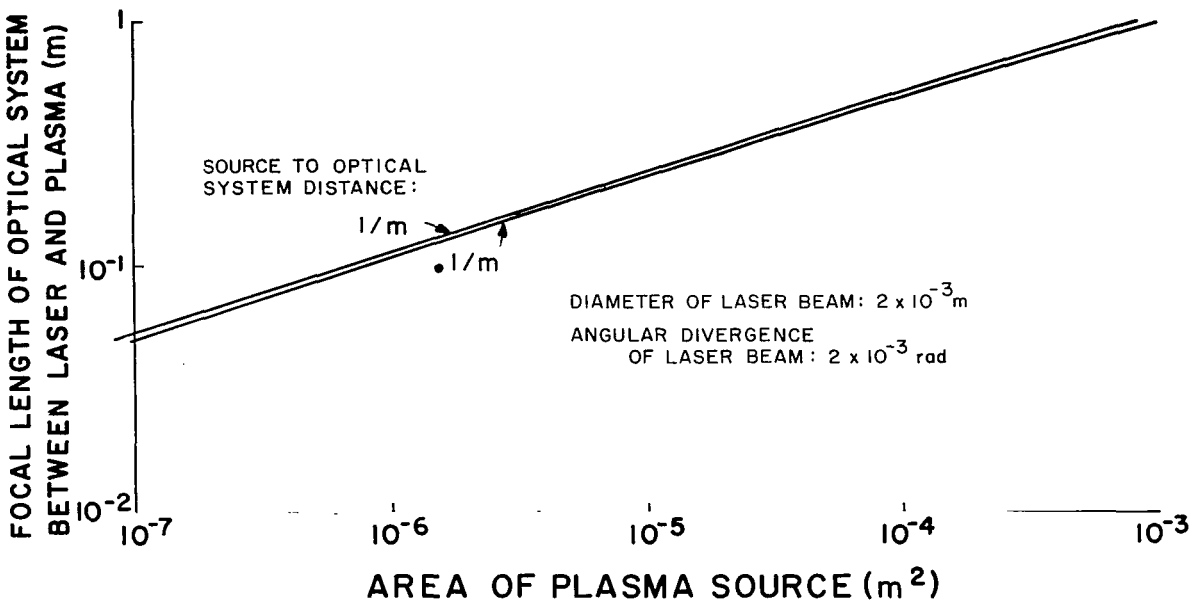

Figure 16.- Area of plasma as a source vs focal length of optical system between laser and plasma.

expressions (9), (10), and (11) into

$$\sin(\theta/2) = (\lambda/4\pi\alpha)\sqrt{ne^2/\varepsilon_0 \kappa T} \quad . \tag{97}$$

The scattering angle is plotted in Figures 18 and 19, in accord with Eq. (97) as a function of particle density for various values of the plasma temperature and for 1.06μ and 10.6μ. It is seen that the scattering angle is quite small at the shorter wavelength for plasma densities that are probably achievable. Such small angle scattering greatly aggravates the problem of shielding the detector from the direct beam of the plasma. Shielding is not a matter that lends itself to reliable calculation and is best solved experimentally.

The power incident on the detector is plotted in Figure 20, in accord with Eq. (44) as a function of the product of the particle density; the focal length of the optical system between the laser and the plasma, and the solid angle subtended by the detector at the plasma for various values of the scattering angle. It will be observed that the scattering is a maximum when the scattering angle is 45 deg, and that the magnitude of the scattering is a quadratic function of the sine of the scattering angle.

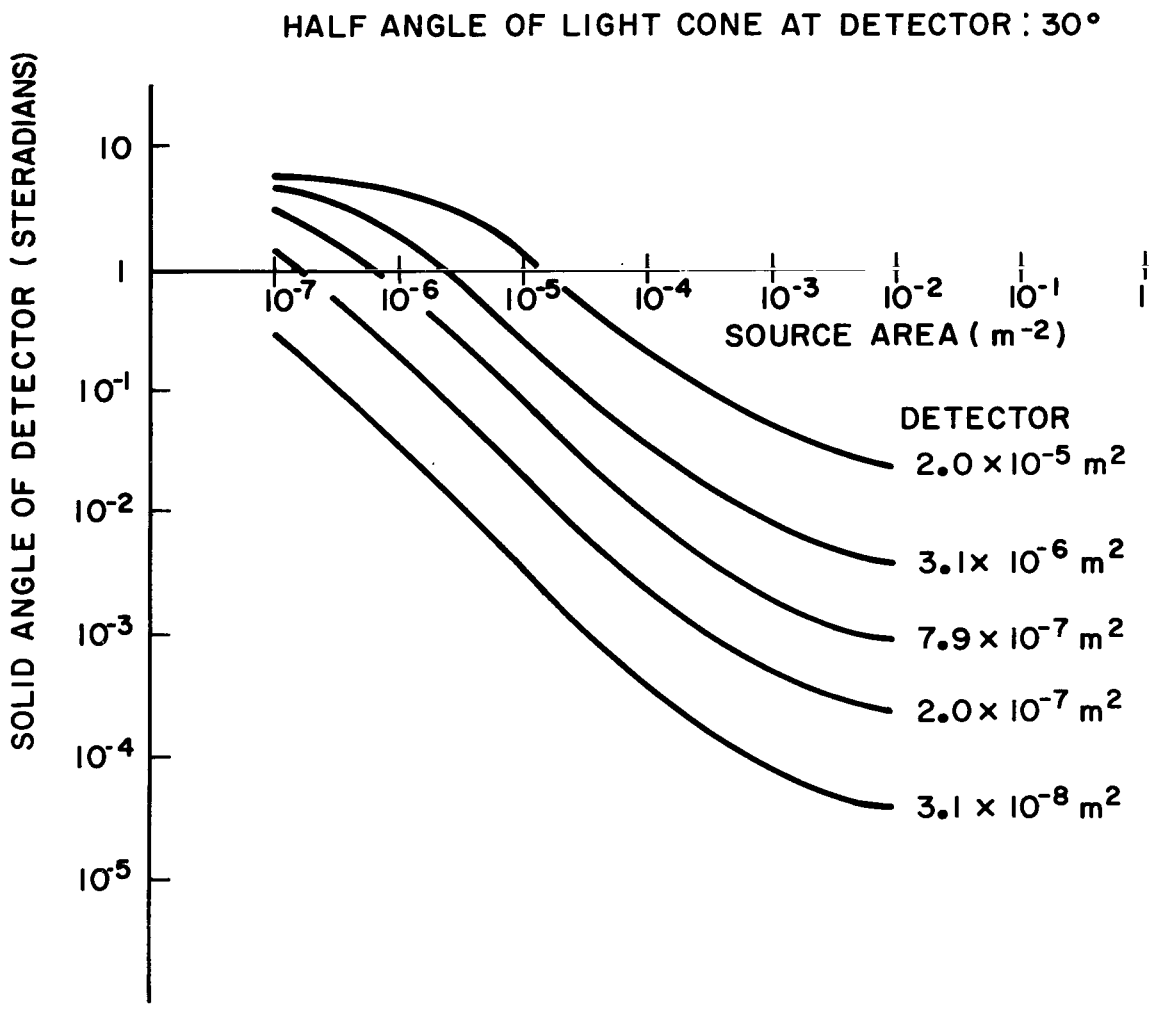

Figure 17.- Solid angle subtended by detector at plasma as a function of plasma area effective for scattering for several areas of the detector.

The argument $hc/(2\kappa T_w \lambda)$ (where T_w is the wall temperature) that appears in expression (92) is plotted in Figure 21 for two wavelengths, 1.06μ and 10.6μ. These wavelengths are those of the NdYAG glass laser and the CO_2 laser. Both lasers can produce considerable power. At longer wavelengths than 10.6μ, the sources are relatively quite weak and experimental techniques are not so well developed as at shorter wavelengths. At wavelengths

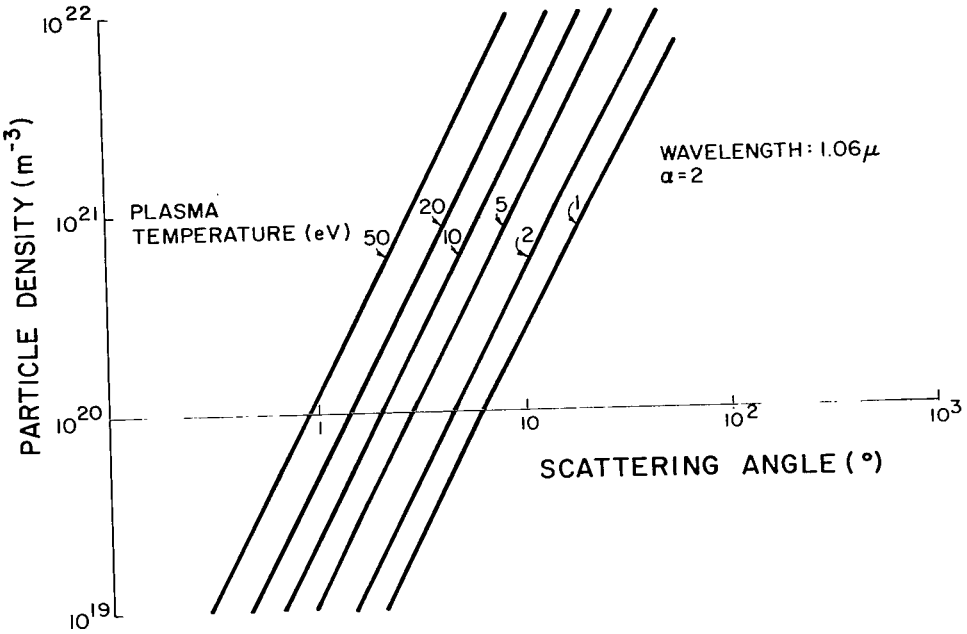

Figure 18.- Scattering angle vs plasma particle density at various plasma temperatures.

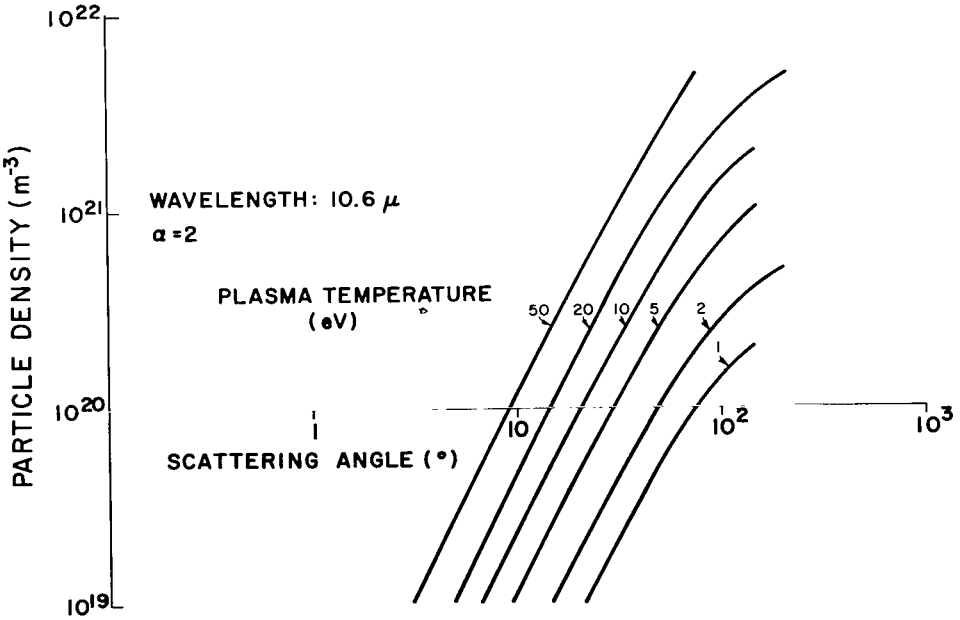

Figure 19.- Scattering angle vs plasma particle density at various plasma temperatures.

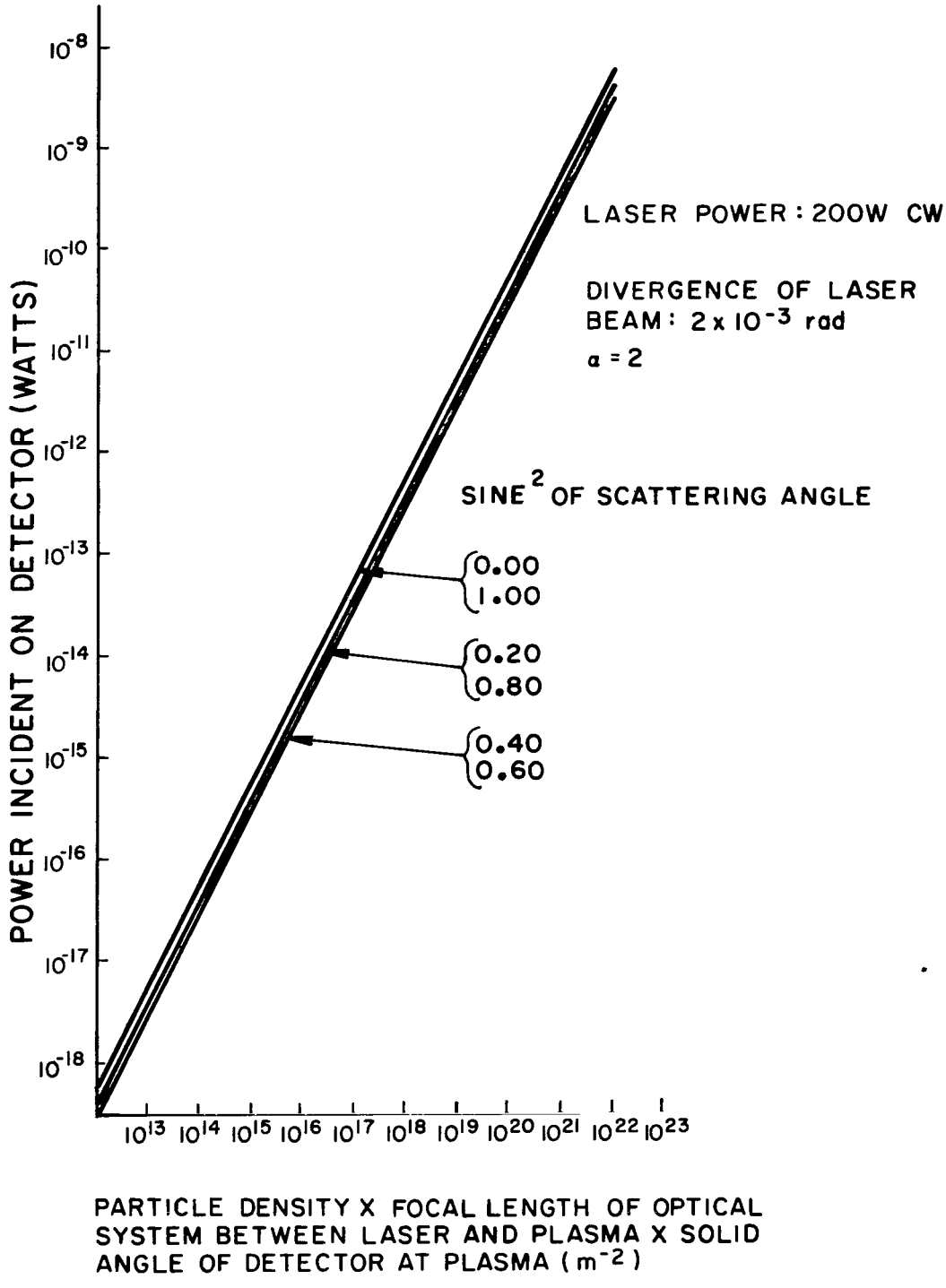

Figure 20.- Power incident on detector as a function of particle density x focal length of optical system between laser and plasma x solid angle subtended by detector at plasma.

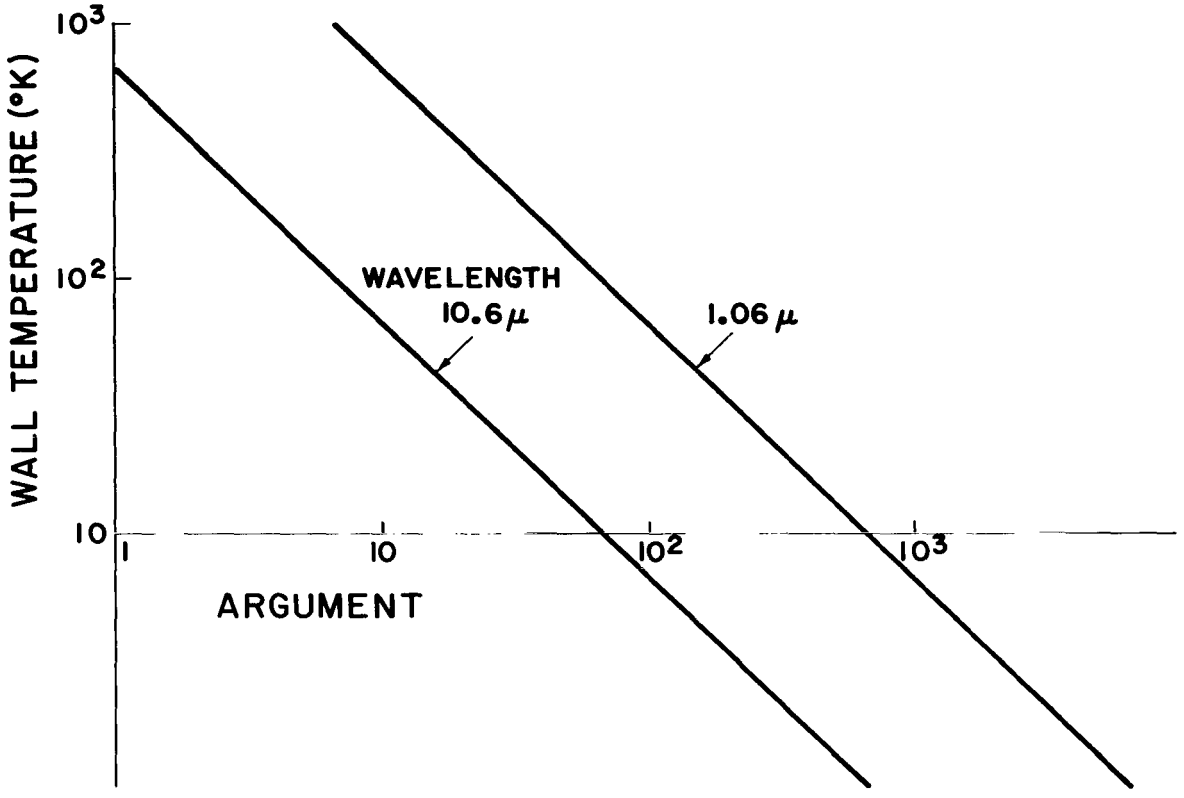

Figure 21.- Argument of exponentials in thermal noise relation vs wall temperature.

shorter than 1μ, the bremsstrahlung becomes prohibitive and the scattering must be observed very much in the forward direction.

In Figures 22 and 23, the thermal noise is plotted in accord with Eq. (92) as a function of the diameter of the detector for various wall temperatures and, in one figure, for a source wavelength of 1.06μ and, in the other figure, for a wavelength of 10.6μ. Thermal noise is far greater at 10.6μ than at 1.06μ, because the Planck distribution reaches a maximum near 10.6μ. Indeed, this fact alone provides strong motivation for performing the experiment at 1.06μ, even though much more power is available at 10.6μ. In either case, the thermal noise may be greatly reduced by cooling the walls seen by the detector. Practically, this suggestion could be implemented by attaching a cylinder, whose axis is the same as that of the detecting system, to the vacuum chamber. The cylinder must be of great enough diameter that the detector sees no part of the wall. The cylinder would then be cooled.

Practical limits are set by the absorption of the components in the optical system between the plasma and the detector. The

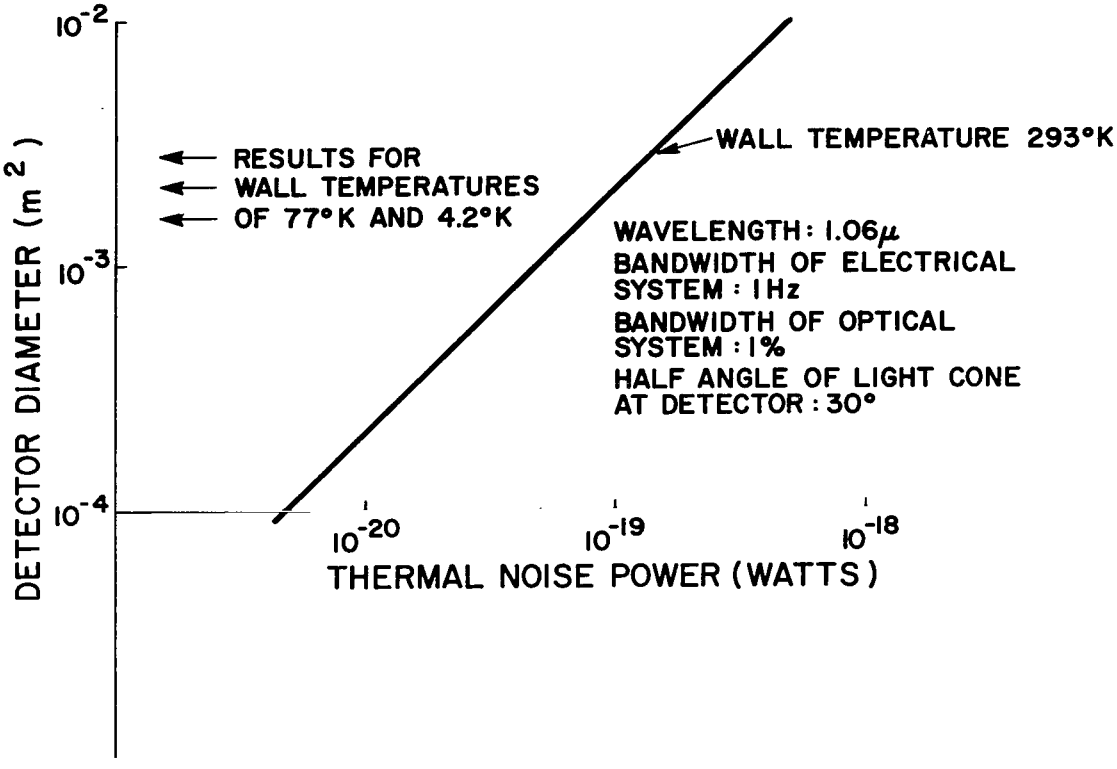

Figure 22.- Thermal noise power as a function of detector diameter for several wall temperatures.

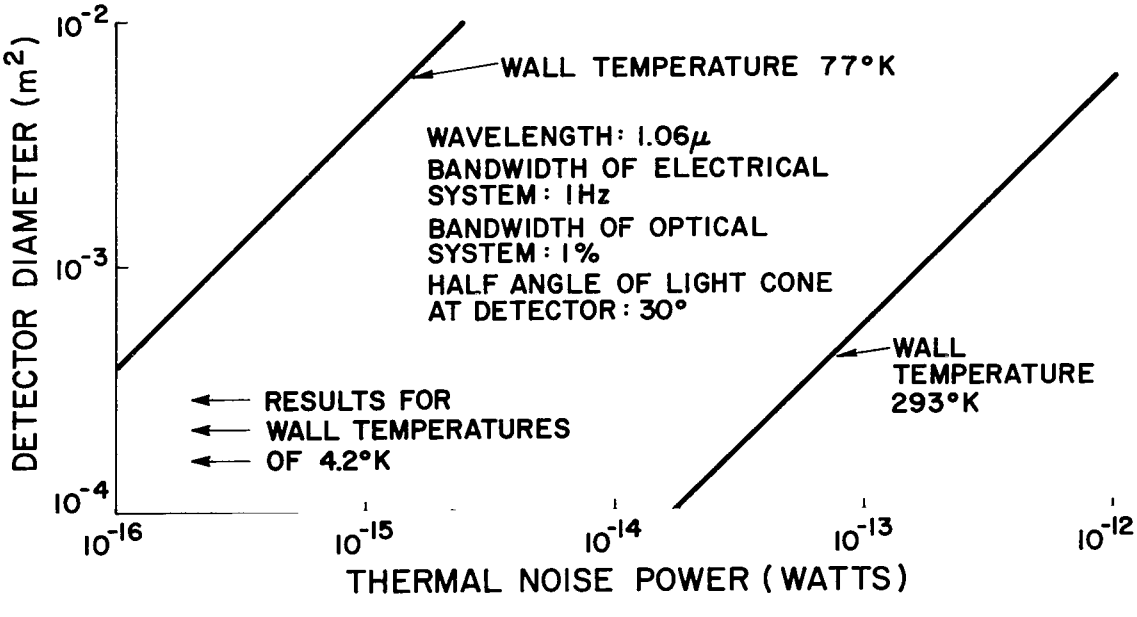

Figure 23.- Thermal noise power as a function of detector diameter for several wall temperatures.

temperature of the wall can be reduced sufficiently that the thermal noise from the optical components between the plasma and the detector dominates the thermal noise of the wall. Of course, these optical components could also be cooled.

The great advantage of working at 10.6μ, as compared with 1.06μ, is that something very effective can be done about reducing the principal factor limiting the signal-to-noise ratio.

We turn next to the noise created by bremsstrahlung. Our problems of presentation are aggravated by an even larger number of independent variables. The bremsstrahlung noise power is plotted in Figures 24 and 25 in accord with Eq. (96) for various plasma temperatures as a function of the product of the particle density squared, the solid angle subtended by the detector at the plasma, the area of the plasma scattering volume projected on a plane parallel to the axis of the light from the laser, and the focal length of the optical system between the laser and the plasma. The results are plotted for 1.06μ and for 10.6μ.

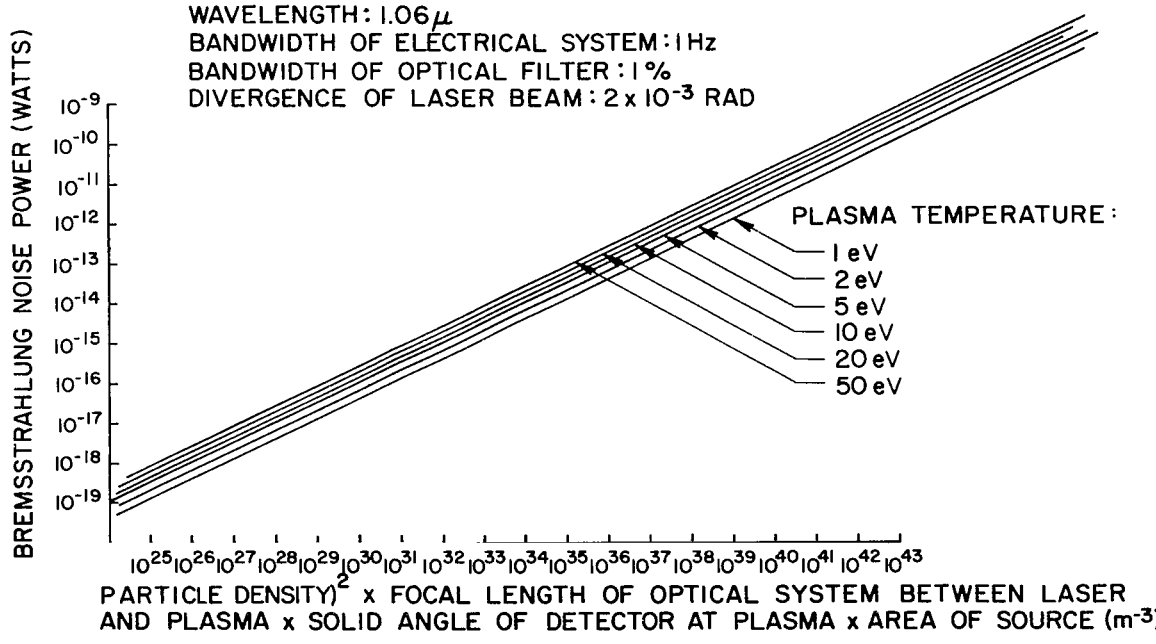

Figure 24.- Bremsstrahlung noise power as a function of the particle density squared x focal length of optical system between laser and plasma x solid angle of detector at plasma x detector area for several plasma temperatures.

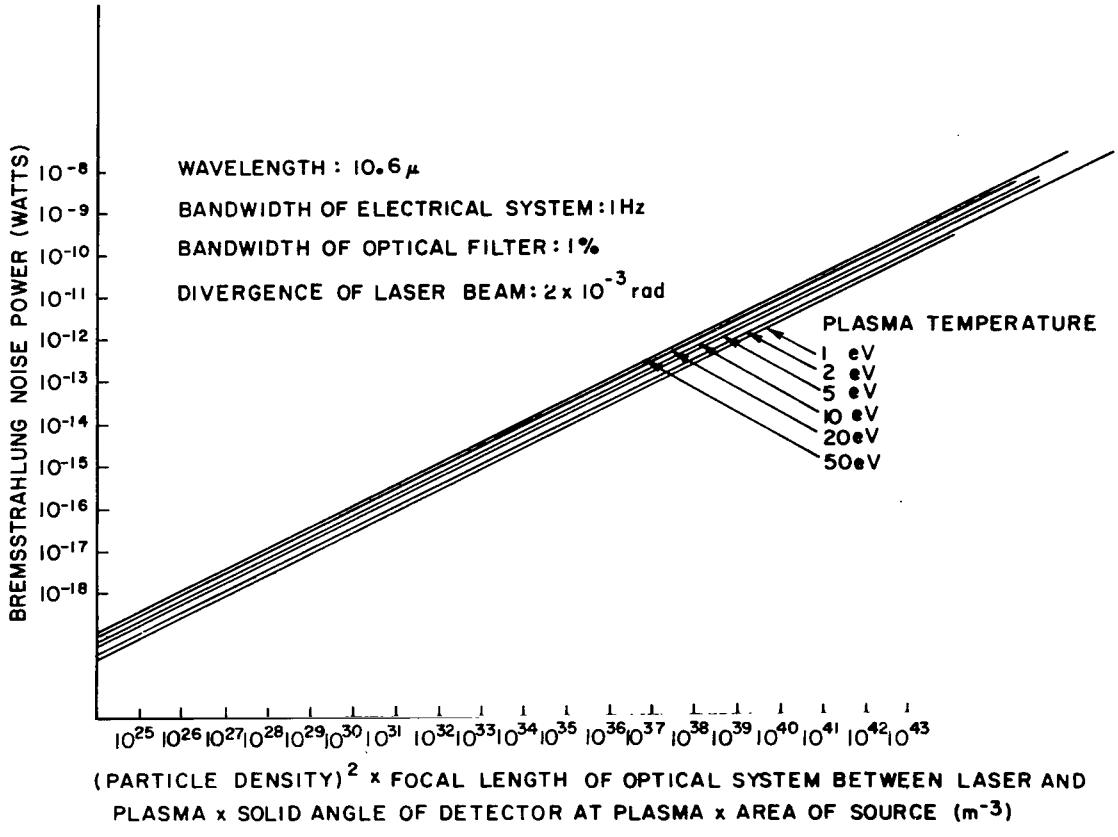

Figure 25.- Bremsstrahlung noise power as a function of the particle density squared x focal length of the optical system between laser and plasma x solid angle of detector at plasma x detector area for several plasma temperatures.

It is observed that the bremsstrahlung power is somewhat higher at 1.06μ than at 10.6μ, other things being equal.

The plasma wavelength is graphed in accord with Eq. (26) as a function of particle density in Figure 26. It is seen from this figure that the cutoff wavelength is much longer than any wavelength at which we might irradiate the plasma. Thus, our radiation will penetrate the plasma.

This frequency determines the location of the satellite lines in accord with Eq. (20). We must now check to determine the kind of filter needed to distinguish these lines from the laser line.

$$\frac{\Delta\lambda}{\lambda} = -\frac{\Delta\omega}{\omega} \approx -\frac{\omega_p \lambda}{2\pi c}\left[1 + \frac{3}{2\alpha^2}\right] \tag{98}$$

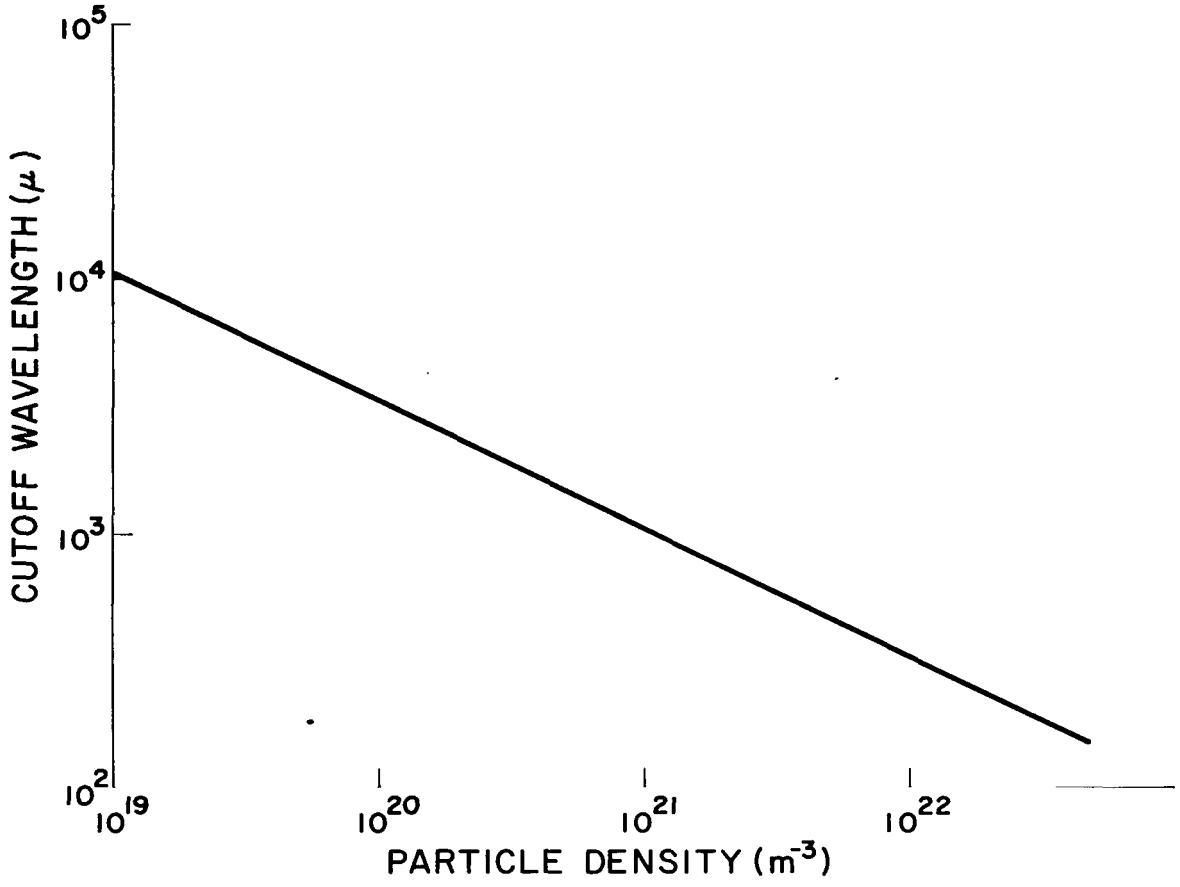

Figure 26.- Cutoff wavelength vs particle density.

The fractional separation in wavelength of the satellite lines is plotted in Figure 27. From this plot, it is seen that it will be necessary to use an interferometer of not very high resolution or a spectrometer to measure the shape of the satellite lines and to distinguish these lines from the central one at the laser frequency.

An example will serve to illustrate the use of the graphs and make more definite some of the results. The numerical results are calculated in the sequence of Figures 15-25.

The numerical results of typical cases are presented in Table V. The first column is a standard with which the results in other columns may be compared. The entries in other columns differing from corresponding ones in the first column are underlined. The entries in this table support the following conclusions:

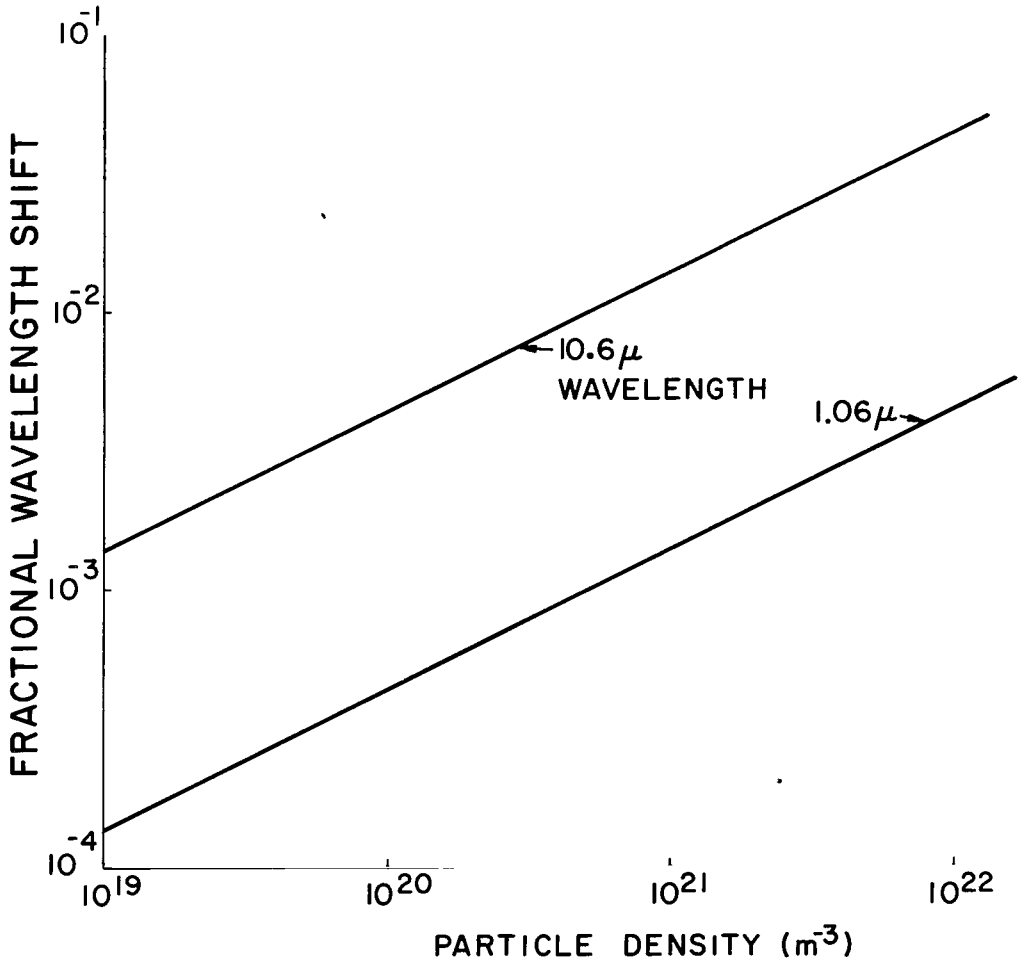

Figure 27.- Fractional wavelength shift of satellite lines as a function of particle density.

* * * * * *

(1) A high plasma density increases the power incident and the signal-to-noise ratio. With a standard set of reference parameters, the thermal noise from the walls of the plasma container is the dominant source of noise. The bremsstrahlung noise is negligible. The scattering angle is also increased from a small one to a value more convenient experimentally.

(2) Reduction of the wall temperature of the plasma reduces thermal noise greatly and greatly improves the signal-to-noise ratio. However, beyond a certain point, the optics, of course, determines when this point is reached.

TABLE V

PARAMETER STUDY OF THE SCATTERING OF LASER RADIATION BY A PLASMA INTO A DETECTOR

Bandwidth of electrical system: 1 cps. Light cone half angle at detector≠30°. Divergence of laser beam: 2×10^{-3} rad. $\alpha = 2$. Fractional bandwidth of optical system at detector: 1%. Diameter of laser beam = 1×10^{-2}m.

Laser power (watts)	200.	200.	200.	200.	200.	200.	10.
Particle density (m^{-3})	$1.\times10^{19}$	$1.\times10^{20}$	$1.\times10^{19}$	$1.\times10^{19}$	$1.\times10^{19}$	$1.\times10^{19}$	$1.\times10^{19}$
Plasma temperature (ev)	1.	1.	1.	5.	1.	1.	1.
Wall temperature (°K)	293.	293.	77.	293.	293.	293.	293.
Focal length of laser-plasma system (m)	0.2	0.2	0.2	0.2	1.	0.2	0.2
Source-optical system distance (m)	0.5	0.5	0.5	0.5	0.5	0.5	0.5
Wavelength (μ)	10.6	10.6	10.6	10.6	10.6	10.6	1.06
Detector diameter (mm)	0.5	0.5	0.5	0.5	0.5	2.	0.5
Power into detector (watts)	5.9×10^{-14}	3.5×10^{-13}	5.9×10^{-14}	5.3×10^{-14}	1.7×10^{-15}	7.2×10^{-13}	2.6×10^{-15}
Thermal noise (watts)	8.5×10^{-14}	8.5×10^{-14}	1.3×10^{-16}	8.5×10^{-14}	8.5×10^{-14}	3.4×10^{-13}	2.4×10^{-20}
Bremsstrahlung noise (watts)	2.9×10^{-18}	2.9×10^{17}	2.9×10^{-18}	7.9×10^{-18}	2.2×10^{-16}	3.8×10^{-16}	1.5×10^{-16}
Scattering angle (°)	21.	77.	21.	9.2	21.	21.	2.1
Signal/Noise (db)	-1.1	6.2	26.6	-2.1	-17.	6.5	12.5

(3) Increases of electron temperature increases bremsstrahlung noise, reduces the scattering angle, and improves nothing.

(4) The focal length of the optical system between the laser and the plasma determines the size of the scattering volume. Increasing this length decreases the power incident on the detector, thus, reducing the signal-to-noise ratio and greatly increasing the bremsstrahlung noise. Be this as it may, the bremsstrahlung noise is still dominated by the thermal noise. Therefore, it is desirable to reduce the focal length of the optics at the input to the plasma as much as the inherent geometry will permit.

(5) Increasing the diameter of the detector rapidly increases the incident power and thermal noise, and very rapidly increases the bremsstrahlung. The signal-to-noise ratio increases somewhat.

(6) Decreasing the wavelength greatly reduces the thermal noise and greatly increases the bremsstrahlung noise. The bremsstrahlung noise increases so much that it dominates thermal noise. The signal-to-noise ratio of the system increases despite the fact that much less power is available. However, the increase is not nearly so great as that which can be attained at the original wavelength by cooling the wall of the plasma container.

It is believed that our choice of particle density is rather conservative and that a much higher value can be achieved. It must also be borne in mind that the improvements listed in Table IV for correlation must be added to the results presented in Table V. At the lower electron densities studied here (10^{19} m^{-3}), the mean free path of electrons in hydrogen is long compared with typical dimensions of the apparatus. At the higher densities (10^{21} m^{-3}), the mean free path is short compared with typical dimensions.

Because of the aberrations of lenses, their absorption, and susceptibility to damage, reflection optics are preferable to refraction optics where reflection optics can be used.

In view of our calculations we conclude that the experiment can be performed. A diagram of the experimental system to perform the experiment is shown in Figure 28.

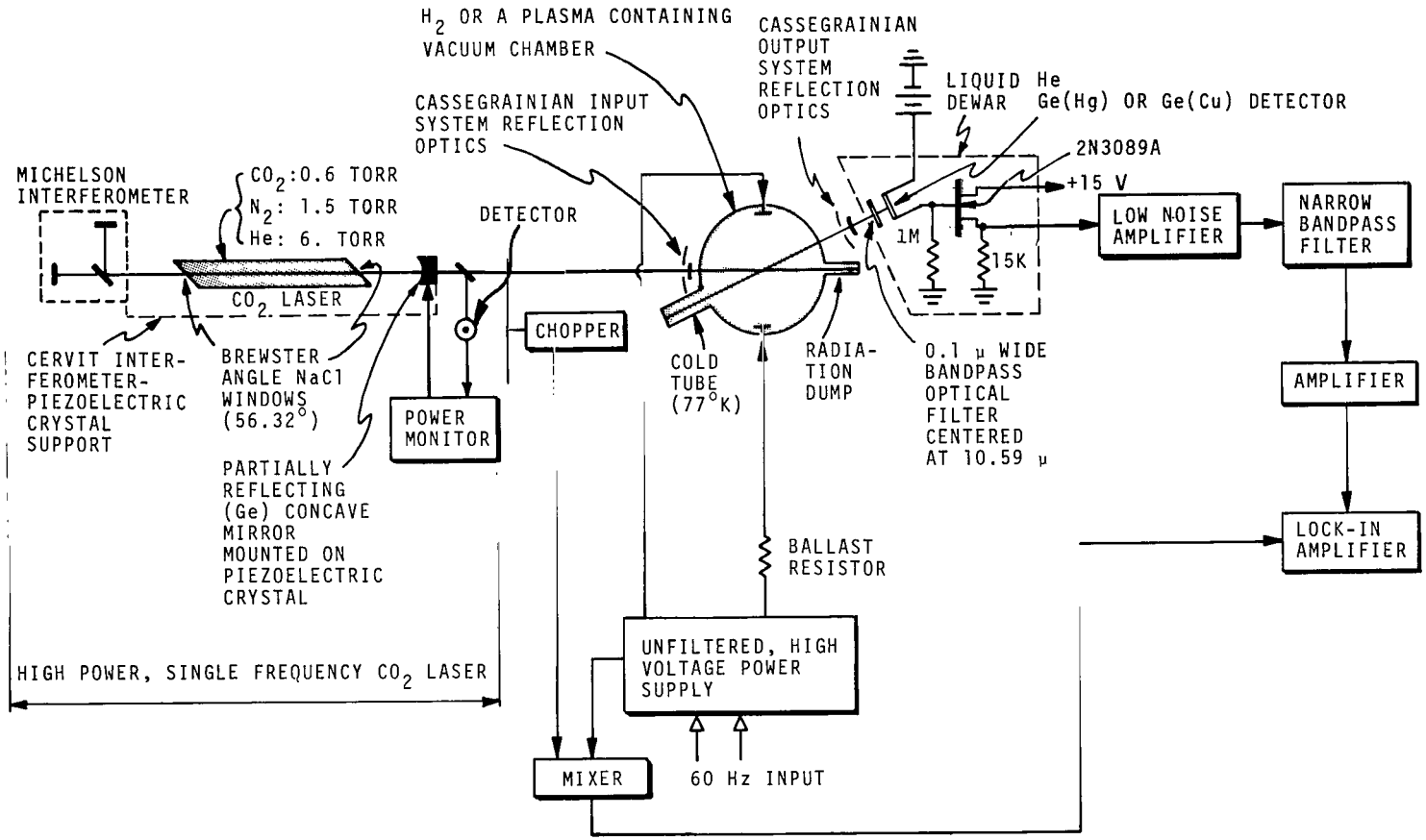

Figure 28.- Experimental system.

REFERENCES

1. Montgomery, D. C., and Tidman, D. A.: Plasma Kinetic Theory. ch. 14, McGraw-Hill Book Co., New York, 1964.
2. Salpeter, E. E.: Electron Density Fluctuations in a Plasma. Phys. Rev., vol. 120, pp. 1528-1535, 1960.
3. Jenkins, F. A., and White, H. E.: Fundamentals of Optics. ch. 3, 6, McGraw-Hill Book Co., New York, 1950.
4. Kruse, P. W., McGlauchlin, L. D., and McQuistan, R. B.: Elements of Infrared Technology. ch. 2, John Wiley, New York, 1963.
5. Whitehouse, D. R.: Understanding CO_2 Lasers. Laser Technology, July 1967.
6. Jenkins, F. A., and White, H. E.: Fundamentals of Optics. ch. 24, McGraw-Hill Book Co., New York, 1950.
7. Jenkins, F. A., and White, H. E.: Fundamentals of Optics. ch. 28, McGraw-Hill Book Co., New York 1950.
8. Garrett, C. G. B.: Gas Lasers. McGraw-Hill Book Co., New York, 1967.
9. Simmons, G. A.: Development of Low-Expansion Glass Ceramic Materials. Optical Spectra, April, May, June, 1967.
10. Tolman, R. C.: The Principles of Statistical Mechanics. ch. 14, Oxford University Press, London, 1938.
11. Smith, R. A., Jones, F. E., and Chasmar, R. P.: The Detection and Measurement of Infrared Radiation. ch. 5, Clarendon Press, Oxford, 1957.
12. Jenkins, F. A., and White, H. E.: Fundamentals of Optics. ch. 5, McGraw-Hill Book Co., New York, 1950.
13. Heisenberg, W.: The Physical Principles of the Quantum Theory. ch. 5, Dover Publications, New York, 1930.
14. Abraham, M., and Becker, R.: Theorie der Elektrizitat, vol. II, ch. A, B. G. Teubner, Leipzig, 1933.
15. Wharton, C. B.: Microwave Diagnostics for Controlled Fusion. Research in Plasma Physics, edited by James E. Drummond, ch. 12, McGraw-Hill Book Co., New York, 1961.
16. Glasstone, S., and Lovberg, R. H.: Controlled Thermonuclear Reactions. ch. 2, D. van Nostrand, 1960.

"The aeronautical and space activities of the United States shall be conducted so as to contribute . . . to the expansion of human knowledge of phenomena in the atmosphere and space. The Administration shall provide for the widest practicable and appropriate dissemination of information concerning its activities and the results thereof."

—NATIONAL AERONAUTICS AND SPACE ACT OF 1958

NASA SCIENTIFIC AND TECHNICAL PUBLICATIONS

TECHNICAL REPORTS: Scientific and technical information considered important, complete, and a lasting contribution to existing knowledge.

TECHNICAL NOTES: Information less broad in scope but nevertheless of importance as a contribution to existing knowledge.

TECHNICAL MEMORANDUMS: Information receiving limited distribution because of preliminary data, security classification, or other reasons.

CONTRACTOR REPORTS: Scientific and technical information generated under a NASA contract or grant and considered an important contribution to existing knowledge.

TECHNICAL TRANSLATIONS: Information published in a foreign language considered to merit NASA distribution in English.

SPECIAL PUBLICATIONS: Information derived from or of value to NASA activities. Publications include conference proceedings, monographs, data compilations, handbooks, sourcebooks, and special bibliographies.

TECHNOLOGY UTILIZATION PUBLICATIONS: Information on technology used by NASA that may be of particular interest in commercial and other non-aerospace applications. Publications include Tech Briefs, Technology Utilization Reports and Notes, and Technology Surveys.

Details on the availability of these publications may be obtained from:

SCIENTIFIC AND TECHNICAL INFORMATION DIVISION

NATIONAL AERONAUTICS AND SPACE ADMINISTRATION

Washington, D.C. 20546